Livrable 1.1: Report on evapotranspiration measurements

Alejandra Leydy, Pierre-Antoine Versini

Projet ANR 17-CE22-0002-01
EVNATURB
Programme JCJC 2017

Livrable 1.1: Report on evapotranspiration measurements

Leydy Alejandra CASTELLANOS DIAZ (HM&Co-ENPC)

Pierre-Antoine VERSINI (HM&Co-ENPC)

Février 2019

Table of Content

Abbreviations

BGW Blue Green Wave
BGS Blue Green Solutions
C_n^2 Structure parameter of the refractive index of air [$m^{-2/3}$]
C_T^2 Structure parameters of temperature [K^2 $m^{-2/3}$]
C_Q^2 Structure parameters of humidity [kg^2 m^{-6} $m^{-2/3}$]
C_p Specific heat at constant pressure
CQM Crassulaceam Acid Metabolism
D Aperture diameter of the transmitter and receiver.
ET Elelectromacnetic
ET Evapotranspiration [mm day^{-1}]
ET_t Evapotranspiration at the time *t*
ET_o Reference Evapotranspiration
e_p Vapour pressure at the leaf surface
e_a Vapour pressure at the canopy air
g Gravitational acceleration [-9.8 m s^{-1}]
h Height of the chamber [m]
I Irrigation [mm day-1]
k Soil thermal conductivity
k_v Von Karman constant [m2 s-1]
λ Latent heat of vaporization of water
L Path-length between transmitter and receiver [m]
LAI Leaf area index [m^2 m^{-2}]
L_{MO} Obukhov length [m]
n Refractive index of air [-]
P Precipitation [mm day^{-1}]
PET Potential Evapotranspiration [mm day^{-1}]
ρ_a Air density [kg m^{-3}]
ρv Absolute humidity [g m^{-3}]
Qe Latent heat/Evapotranspiration flux [W m^{-2}]
Qh Sesible heat flux [W m^{-2}]
Qr Surface runoff or overflow
σ_x^2 Variance of natural logarithm of intensity fluctuations [-]
θ Moisture content [-]
θ_{FC} Moisture content at field capacity [-]
θ_{MAX} Maximum moisture storage capacity [-]
θ_t Moisture content at the time *t* [-]
$\Delta\theta$ Average moisture content [-]
R_n Net radiation [W m^{-2}]
r_a Aerodynamic resistance
r_s Surface resistance
r_e Canopy external resistance
r_i Canopy internal resistance
T_0 Initial temperature [K]
T Air temperature [°C]
T_* Temperature scaled [K]
t Time [s, day]
U_2 Wind speed [m s^{-1}]
u_* Friction velocity [m s^{-1}]
z_{LAS} Effective height of the scintillometer beam [m]
z_s Depth of the soil [mm]
γ Thermodynamic psychometric constant [Pa $°C^{-1}$]
Δ Slope of the saturation vapor pressure-temperature relationship [Pa $°C^{-1}$]

ABSTRACT

Understanding the physical and thermal processes that govern Bleu Green Solutions (BGS), such as evapotranspiration (ET), is one of the challenges of urban hydrology to determine their possible impacts to mitigate urban heat islands. Evaluate the ET process in BGS, specifically in the green roof installed in front of the Ecole de Ponts, is the main objective of this work. Hence, three different direct and indirect methods have been tested and compared to estimate ET: (i) a soil moisture content measurement via a wireless sensors network and by using the water balance, (ii) an absolute humidity measurement provided by a dynamic transpiration chamber, and (iii) an indirect method based on the energy budget and by using a scintillometer to assess the sensible heat flux. In a second time, the spatial and time variability of the measured ET flux will be evaluated by multifractal tools, allowing to assess this hydrological process through different scales.

1. INTRODUCTION

Urban land development and climate change generate real challenges for the sustainable development of the cities. These issues include the modification of the water cycle, the increase of temperature -resulting in urban heat islands (UHI) -, the increase of intense events as drought and flood (due to the overload of the drainage system) and pollution. UHI is a phenomenon where a significant difference in temperature during the night can be observed within a city in comparison with its surrounding sub-urban/rural areas (O'Malley et al., 2015). In consequences, alarming effects in terms of energy consumption and health -especially in summer- have been observed. This phenomenon is caused by the changes in urban surfaces, which have altered the radiative, thermal, moisture and aerodynamic properties of the environment (Kolokotroni and Giridharan, 2008).

However, during the last years, thanks to environmental awareness and the need to adapt the cities to climate impacts, a paradigm shift to make urban environments more sustainable and resilient has been proposed by public authorities, scientific community and international environmental organizations. This new paradigm defines several sustainable adaptation strategies and proposes to (re)introduce natural soil processes in the cities, such as infiltration and evaporation processes, by the increasing presence of green areas.

Different Blue Green Solutions (BGS), such as green roofs, vegetated swales, infiltration trenches, storage reservoirs etc., have been adopted to make cities more resilient and to promote environmentally friendly spaces (Besir and Cuce, 2018). These solutions can act as storm-water management tool, to compensate the cities' carbon emissions, improve the air quality, reduce the energetic consumption, protect the biodiversity and increase the public space (Cascone et al., 2018; Marasco et al., 2015; Versini et al., 2016; Wadzuk et al., 2013).

Indeed, green roofs have been widely appreciated as one of the most interesting solutions to reduce the water volume in the drainage systems (through the effect of water retention and evaporation) and to delay the runoff (Mentens et al., 2006, Versini et al, 2016). Green roofs can also be used to mitigate the effects of UHI in urban areas through increasing evapotranspiration (Mentens et al., 2006; Wadzuk et al., 2013). A study from the University of Villanova in the United States, reported that 68% of total precipitation fell in the green roof was lost by evapotranspiration (Wadzuk et al., 2013). This structures have the ability to moderate temperature changes within buildings (De Munck et al., 2013), by the action of the vegetated substrate which protects the roofs from the direct penetration of the solar radiation and by the increase of the evapotranspiration, which generate a cooling effect (Barrio, 1998; Besir and Cuce, 2018). A model in Toronto (Canada) concluded that the implementation of this BGS on the 50% of roofs, produces a temperature reduction close to 2°C (Oberndorfer et al., 2007).

In order to understand the benefits of green roofs with the variable climatic conditions, it is necessary to know and interpret the physical and thermodynamical processes that lead these green structures. For this reason, a large part of the ANR EVNATURB project is focused on the estimation of the ET flux and its space and time variability through scales.

1.1. The ANR EVNATURB project

The ANR EVNATURB project (2018-2022) "*Evaluation des performances écosystémiques d'une renaturation du milieu urbain"* aims to develop an operational platform to assess some

of the eco-system services (i.e. storm water management, cooling effect, or biodiversity conservation) provided by BGS at the district scale, and to promote the re-naturation of cities (HM&Co, 2017). This project has several objectives:

I. Coupling hydrology, thermic, urbanism, biodiversity and the corresponding ecosystemic services;
II. Characterizing the spatio-temporal variability of the related processes over a wide range of scales by (i) the implementation of a complex, portable and high resolution monitoring, and (ii) the use of adapted analysis and modelling tools;
III. Developing a scientific network devoted to BGS monitoring and contribute to expand knowledge and fulfill the lack of feedback concerning the functioning of existing BGS;
IV. Characterizing the implementation of BGS infrastructures by taking into account local socio-environmental stakes and constraints, and define some quantitative indicators relevant for the development project (certification, labeling, compliance with local regulations, continuity with surrounding biodiversity, etc.).

This deliverable (1.1) is part of Objective II and concerns the monitoring of the ET process.

1.2. The ENPC Blue Green Wave (BGW)

To tackle this issue, the EVNATURB project aims to monitor, understand and reproduce thermal and hydrological processes, such as infiltration and evapotranspiration, in vegetated infrastructures. One of the pilot sites is the French Green Wave located in front of Ecole des Ponts ParisTech (Champs-sur-Marne, France). Since 2013 and the Blue Green Dream (BGD) project (Maksimovic et al., 2013), several measurement campaigns have been carried out on this large (1 ha) wavy-form vegetated roof (Versini et al., 2018). The Blue Green Wave represents a pioneering site (Figure 1) where an initially decorative design project has been transformed into the BGD research oriented one.

Figure 1. The Blue Green Wave at Champs-Sur-Marne

Two types of vegetation are planted: green grass and a mix of perennial planting, grasses and bulbous (see Table 1). They are based on a substrate layer (210 mm depth for the grass, 280 mm depth for the mix of vegetation respectively), a filter layer (synthetic fiber) and a drainage layer (polystyrene). The substrate is composed of volcanic soil completed by organic matter (around 13%) and is characterized by a density of 1446 g/L and a total porosity around 60%.

Construction type	Vegetated mat
Year build	2013
Localization	
Roof area (ha)	1 ha
Substrate depth (mm)	- 210 (green grass) - 280 (mix)
Plants species	- Green grass - Mix of perennial planting, grasses and bulbous
Type of substrate	Volcanic soil
Substrate density (g/L)	1446
Substrate porosity (%)	60

Table 1. Green Wave Characteristics

The site is also equipped with several water storage capacities that strongly encourage future development of multifunctional green spaces. These capacities store excess volumes of water during heavy storms and release them afterwards. In details, part of the green roof supplies a stormwater tanks, which is especially used for the sprinkle of the roof's vegetation layer. Remaining green roof and impervious areas are connected to a large retention basin, which has been oversized. Indeed, for now in France, there is no guideline concerning basin sizing that takes into account the retention properties of green roof.

2. OBJECTIVE

This study aims to measure as precisely as possible and analyze the thermo-hydrologic behavior of green roofs, and particularly the evapotranspiration flux (latent heat flux) on the BGW. Evapotranspiration represents a key component as it makes the link between the water balance and the energy budget. In consequence, it conducts the ability of the structure to mitigate urban heat island (cooling effect) and to act as a stormwater management tool by its retention capacity.

3. METHODOLOGY

In order to achieve this objective, two basic steps were established. First, an exhaustive review was planned. It concerned the thermo-hydric balance of vegetated roofs, the different methods used to estimate ET and the factors that may influence its measurement. The second stage was the development of several strategies, which has been carried out through three ET measurements:

1. A wireless sensor network to measure water content and temperature, which makes possible the capture of the space-time variability of retention and infiltration processes. This network provides some punctual measures over a heterogeneous surface.
2. A dynamic transpiration chamber, which allows analyzing the gas exchanges, in particular water vapor. This device measures a punctual ET rate over a surface considered as homogeneous.
3. A scintillometer specially adapted to measure sensible heat flux over a large and heterogeneous land surface at high resolution. In addition with other sensors, it makes possible the estimation of the latent heat flux (proportional to ET).

Those methods provide measurements of ET at different spatial scales based on the thermo-hydric balance of the green roof, which allows to analyze the results of each method and the ET flux dynamics. They have been tested on the Green Wave located at ENPC.

4. LITERATURE REVIEW

4.1. Green roofs

Green roof is a BGS based on the use of buildings roofs as a vegetation support, achieving numerous environmental benefits such as reduced storm-water runoff, thermal benefits, noise reduction, reducing air pollution and providing wildlife habitat and biodiversity enhancement (Stefferud, 2016). Green roofs also known as ecological roofs, living roofs or garden roofs, are the first manifestations of plant systems in the cities, as the Hanging Garden of Babylon. While modern green roofs originate from Germany in the 20th century, and were put in place to mitigate the harmful physical effects of solar radiation in the roof structure (Oberndorfer et al., 2007).

A green roof consists of a set of different layers: vegetation, growing medium, filter, drainage material, root barrier, water proofing membrane and insulation layer (Berretta et al., 2014; Besir and Cuce, 2018; Oberndorfer et al., 2007). The upper outer layer lays on the vegetation in a growth medium, denominated substrate (Berretta et al., 2014; Cascone et al., 2018). The natural layer (vegetation and substrate) is installed on a filtration layer, followed by a drainage layer; an anti-roof barrier and finally by the impermeable membrane. The substrate is usually composed by a mixture of organic and inorganic materials, such as sand, expanded clay, vermiculite, perlite, grave, crushed brick, peat, organic matter and soil.

Green roof classification varies among scientists due to the substrate depth, type of vegetation, maintenance, cost, and need for irrigation (Cascone et al., 2018; Oberndorfer et al., 2007; Wadzuk et al., 2013). However, the following classification is usually used. It groups together these characteristics and makes possible to identity three categories of roofs (Besir and Cuce, 2018) (see Figure 2):

- Intensive: The substrate depth is the most important (15-45 cm or higher); it needs a high level of maintenance and regularly irrigation.
- Semi-intensive: The soil layer has a medium depth substrate (12-25 cm); it needs periodic maintenance and irrigation.
- Extensive: It has the thinnest substrate layer (5-20 cm), followed by small vegetation; its maintenance cost is very low.

	Extensive green roof	Semi intensive green roof	Intensive green roof
Maintenance	Low	Periodically	High
Irrigation	No	Periodically	Regularly
Plant communities	Moss-Sedum-Herbs and Grasses	Grass- Herbs and Shrubs	Lawn or Perennials, Shrubs and Trees
Cost	Low	Middle	High
Weight	60–150 kg/m^2	120–200 kg/m^2	180–500 kg/m^2
Use	Ecological protection layer	Designed green roof	Park like garden
System build- up height	60–200 mm	120–250 mm	150–400 mm underground garages ≥ 1000 mm

Figure 2. Classification of green roofs according to the type of use (Besir and Cuce, 2018).

4.2. Green Roof Evapotranspiration

In urban areas, the vegetation has been largely replaced by shading and impervious surfaces as asphalt roads and buildings (Oberndorfer et al., 2007). These types of surface represent one of the main responsible of greenhouse gas emission. In particular, buildings change the flow of energy and matter in urban ecosystems and consequently lead to the production of UHI (Cascone et al., 2018).

The modification of the urban microclimate has a high influence on ET, phenomenon that represents an important component of the water balance with the establishment of green spaces (Marasco et al., 2015). For instance, 30 to 70% of the precipitations (depending on the season) returns to the atmosphere through ET (Guyot et al., 2009). Also, ET might have positive and negative effects in indoor conditions (Besir and Cuce, 2018). Vegetation ET increases the ambient moisture, which raises the humidity inside of buildings (Wang et al., 2014) and sharpens the consequences of UHI. However, as our understanding over the influence of ET in the surface energy flux is reduced, it is frequently neglected or simplified in the urban hydrological models.

ET is the water vapor flux transferred from the terrestrial surface to the atmosphere under the action of gravity and solar energy (Marasco et al., 2015; Poë et al., 2015). This physical phenomenon is the result of combined actions between the soil evaporation and the plant transpiration (Brown, 2014). There are three key and interdependent processes, which take place during the ET phenomena. First, there is an ascending capillary flux of water from the lower to the higher soil horizons. In second place, there are evaporative loses from the soil surface to the atmosphere. Finally, the transpiration occurs from the soil water by the plants (Poë et al., 2015).

Evaporation E: is the process of transforming liquid water into vapor. The evaporation may come from interception, meaning that some of the precipitation is intercepted by the vegetation and returned to the atmosphere. There may also be a depression storage from a temporary pond on the roof surface depending on the type of vegetation and the slope. Surface evaporation may also occur, meaning that the water stored in the soil moves towards the surface and then evaporates (Stefferud, 2016).

Transpiration T: consists in the process whereby the plant's root system absorbs the interstitial water, transporting it through the xylem to stomatitis cavities in the leaf where water evaporates under the action of solar energy. Transport from the roots to the leaves is given by the potential differential, due to the water deficit in the leaf cells, which generates a suction force transmitted to the root (Brown, 2014; Poë et al., 2015). Stomata are responsible of most of the water loss by green roof plants. Stomata are tiny pores in the leaves through which enter the gases needed for photosynthesis such as CO_2, O_2 or water vapor (Tabares and Srebric, 2012).

Factors influencing ET of a green roof.

ET primarily results of the solar energy, although can be influenced by the site environmental conditions (e.g. surface albedo, aerodynamic roughness, boundary layer humidity profile and available substrate moisture) and the proprieties of the planted vegetation. However, the urban green spaces ET is affected by specific properties, including small scale, vegetation heterogeneity, substrate depth and its proprieties (e.g. porosity), the underlying surfaces and the uncertainly about the availability of moisture in the substrate (Marasco et al., 2015).

The soil moisture is one of the most influential factors affecting ET. When the soil is saturated, the water supply for ET is significant and the process is energy limited. Gravitational forces, in addition to loss through ET, enforce water to leave the soil matrix until the soil reaches a maximum moisture deficit while it becomes increasingly more difficult for ET to occur (Marasco et al., 2015; Wadzuk et al., 2013).

In addition, to soil moisture, the factors that affect ET are the type of vegetation, its stage of development and the meteorological conditions (Brown, 2014; Marasco et al., 2015; Tan et al., 2017). The stage of development of the plant refers to its active growth and size. Small plants (dormant or latent) use less water, while large plants in active growth require much more.

The type of plant may have more or less influence on ET, due to its physiological characteristics. Native plants suitable for dessert - that adopt Crassulaceae Acid Metabolism (CAM) - need less water. CAMs are plant species that are generally more drought tolerant than other species. They have the ability to open their stomata to metabolize during the nights when temperatures are colder. As a result, there are lower evaporation losses than plants that transpire during daylight conditions (Poë et al., 2015; Tan et al., 2017).

Additionally, the meteorological conditions such as solar radiation, air temperature and wind force ET (Brown, 2014; Poë et al., 2015). The rate at which these parameters force ET, depends on the characteristics of the substrate (i.e. field capacity and permeability), as well as the additional storage moisture capacity in the vegetation layer and the physiological response of the plant to moisture content (Poë et al., 2015; Tan et al., 2017).

4.3. Thermo-Hydric Balance of Vegetated Roofs

The different exchanges between the natural layer of the green roof (plants and substrate) and the environment imply a transfer of energy and mass in thermal and hydrological terms which control the performance of the roof.

Evapotranspiration estimation is a main issue studied by the hydrologists, who have developed several direct and indirect methods through monitoring and modeling approaches (see detail sin next section). Indirect methods are usually based in the conservation of mass (water in this case) and the energy balance. The primary link between the energy and water balance equations is the evapotranspiration term in both equations (Lakshmi et al., 2003). The hydrologic characteristics of green roofs are critical aspects, that strongly influence the energy (thermal) balance (Tan et al., 2017), as well as their configuration and the climatic context of the green roof site (Malys et al., 2014).

Both thermal and water balance calculate ET based on the energy flux components and the water distribution in the natural layer. In addition, experimental studies on pilot roofs have highlighted that heat and water transfer within the vegetal and soil layers are similar to those within the natural ground surfaces, except for specific limit conditions (De Munck et al., 2013). For this reason, ET can be expressed in two different ways:

- Energy flux (Q_e), used by meteorologists in W/m^2.
- Mass flux (ET), corresponding to the height of water lost by soil evaporation and plant transpiration over a period of time [mm/d or in/d], similar to precipitation and commonly used by the hydrologist (Brown, 2014).

Both definitions are linked by the following Equation (1):

$$Q_e = ET \cdot \lambda \quad [W\ m^{-2}] \qquad (1)$$

Where ET represents the flux density of water molecules, meaning the mass of water transported per unit time and area [kg $m^{-2}s^{-1}$], λ is the energy required to vaporize a unit of water mass (1 kg of water ~2.45 x10^6 Jkg^{-1}), and Q_e is the Latent heat flux [mm d^{-1}].

Energy Budget

Evapotranspiration is a process governed by the energy exchanges at the vegetation and soil surfaces. The change of state (liquid to vapor) requires a significant amount of energy. Consequently, ET is delimited by the amount of energy available and it is possible to calculate it by the principle of energy conservation.

In green roofs like in traditional roofs, the energy conservation results in a balance (Equation 2 and Figure 3) dominated mainly by the radiative force from the sun (Marasco et al., 2015), contrasted by the fluxes of latent heat (evapotranspiration) and sensible heat (convection) from soil and plant surfaces, and combined with conduction of heat into the soil substrate (De Munck et al., 2013). The flux transferred horizontally, by advection, are ignored, and photosynthesis, divergence and storage terms are neglected.

$$R_n = Q_g + Q_e + Q_h \qquad (2)$$

Where R_n is the net radiation in the surface [W m^{-2}], Q_g is the soil heat flux [W m^{-2}], Q_e is the latent heat flux [W m^{-2}] and Q_h is the sensible heat flux [W m^{-2}]. All terms can be either positive or negative, depending on the flux direction. For example, the sensible heat flux is negative when it delivers energy to the roof surface, and positive when it removes energy from the roof (Ayata et al., 2011). These components are explained in details in the following.

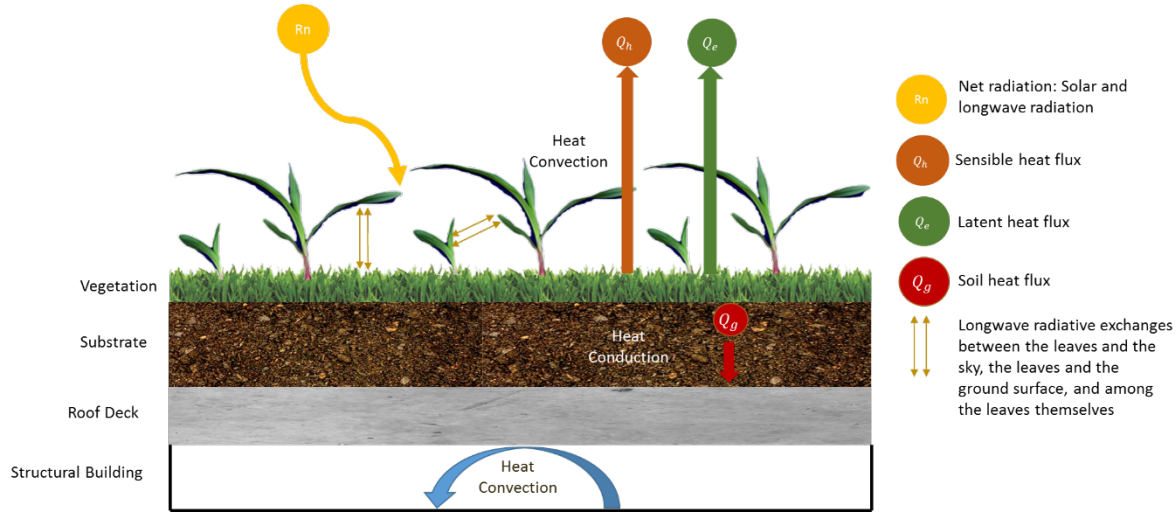

Figure 3. Energy balance in a green roof.

Net Radiation (Rn): it is the most important component of the surface energy. It corresponds to the difference between incident and reflected radiations. The incident radiation includes the solar radiation reaching the soil surface and the longwave radiation. The amount of solar radiation reflected by the soil depends on the surface albedo coefficient (α), which consists in the fraction of the incident sunlight that the surface reflects back into the atmosphere, while the longwave radiation varies by the emissivity of the soil (ε) and typical values are 0.90-0.98 (Tabares and Srebric, 2012). Both solar and longwave radiation exchanges are a function of atmospheric conditions, especially cloud conditions.

Sensible heat flux (Q_h): it is the energy flow exchanged through the atmosphere from one place to another and the convection is its transport mechanism (transfer of air masses at different temperatures). Consequently, measurement of the sensible heat is complex and cannot be easily obtained. Q_h requires accurate measurement of temperature gradients above the surface.

Latent heat flux (Q_e): it is directly related to the water vapor and represents the evapotranspiration or water vapor flux. Thus, Q_e is the energy needed for the evaporation process.

Soil heat flux (Q_g): it is the energy propagation trough conduction (transfer of kinetic energy between molecules), between the plants surface and the soil. The intensity of the conduction is a function of the medium density, the mobility of the molecules and the thermal gradients. Heat flow in soil can be considered analogous to heat flow in a solid to which Fourier's Law is applied. The rate of heat transfer through a specific material is governed by its thermal conductivity k (the higher the thermal conductivity, the greater the heat transfer (Becker and Wang, 2011):

$$G = -k\frac{\partial T}{\partial z} \tag{3}$$

Where, k is the thermal conductivity of the soil [W m^{-1} K^{-1}] and $\frac{\partial T}{\partial z}$ is the vertical temperature gradient [K m^{-1}] of the soil layer.

However, there is a great difficulty in obtaining accurate k measurements under field conditions, because it is mainly a function of the soil water content and substrate type. In fact, various authors have studied the relation between k and θ (See Table 2):

Table 2. Relation between soil thermal conductivity and volumetric water content.

Becker and Wang, 2011	$k = 0.8\ [\mathrm{W\,m^{-1}K^{-1}}]$ with $\theta = 0$	Composition of green roof substrate: 75% shale, 10% compost and 15% sand.
Evett et al., 2012	$k = \propto C_v$ $k \sim 0.4 - 1.2\ [\mathrm{W\,m^{-1}K^{-1}}]$	Thermal conductivity of a mineral soil with negligible organic matter ($\propto$ is the diffusivity [m^2 s^{-1}] and C_v corresponds to the volumetric heat capacity)
Tabares and Srebric, 2012	$k = a_1 + a_2 \cdot \theta$	Thermal conductivity of a green roof substrate. Substrate based on expanded clay: $a_1 = 0.16$ and $a_2 = 0.51$ Substrate based in expanded shale: $a_1 = 0.2$ and $a_2 = 1.4$
Gagliano et al., 2016	$k = 1.0\ [\mathrm{W\,m^{-1}K^{-1}}]$	Green roof substrate composed by a mixture of peat, pumice, mineral aggregates and other soil granules.
Ren et al., 2017	$k = 45.318 \cdot \theta^{0.6619}$	Silty loam surface soil from a cultivated land in Shanxi Province, Chine
Yang et al., 2018	$k = 0.35\ [\mathrm{W\,m^{-1}K^{-1}}]$	Properties of green roof: Thickness= 0.1 [m] $\theta = 0.3$ [m^{-3} m^{-3}]

The surface temperature determines the fluxes of outgoing longwave, sensible, and ground heat. The magnitude of these fluxes determines the latent heat flux. Hence, understanding the relationship between soil moisture and surface temperature makes possible the evaluation and prediction of evapotranspiration in the green roof (Lakshmi et al., 2003; Stefferud, 2016).

Water Budget

Green roof performance is related to the ET rate, which is one of the factors delimiting the storage availability within soil for the retention of additional rainfall (Wadzuk et al., 2013). In terms of hydrological transfer, a green roof surface behaves like any other natural surface except that the hydrological characteristics of green roof soil-forming materials are different, and that the water drained out of a green roof is lost "in favor of" the rainwater network (De Munck et al., 2013).

ET is an essential component of the green roof water balance $ET = P + Ir - Qr - \Delta S$ *(4)*, but this process is still poorly quantified because it is highly variable in time and space (Malys et al., 2014; Wadzuk et al., 2013).

$$ET = P + Ir - Qr - \Delta S \quad (4)$$

Where, P is the precipitation [mm], Ir is the irrigation water [mm], ΔS is the stored water in the matrix of the soil [mm] and Qr corresponding to the surface runoff or overflow [mm].

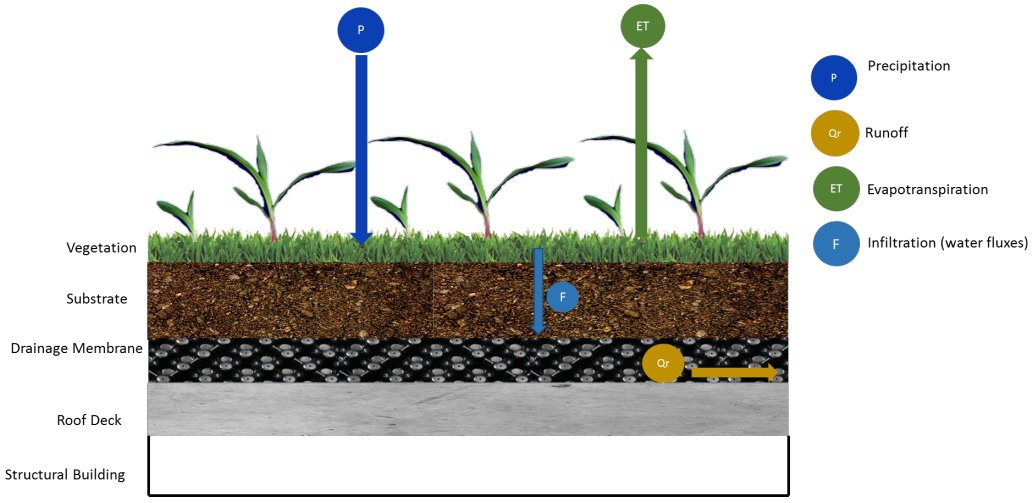

Figure 4. Water Balance in the green roof.

ET via the water balance consists of assessing the incoming and outgoing water flux from the soil layer over a period of time. Precipitation and irrigation provide water to the soil layer, which can be lost by runoff, whereas the ET is lost water as vapor into the atmosphere.

4.4. Evapotranspiration estimation

The estimation of ET is a complex process, since it involves a continuous control of a large number of physical, meteorological and plant cover parameters. Consequently, several direct and indirect methods have been defined for its calculation. On one hand, direct methods include Lysimeter, which measures the variations of soil humidity; or transpiration chamber, which quantifies the changes of water vapor concentration from plan canopies. On the other hand, indirect methods include the use of micrometeorological techniques such as Eddy

Covariance EC, (which provides measurements of the transfer of land surface turbulent fluxes into the atmosphere (Valayamkunnath et al., 2018)), Surface Energy Balance and Field Water Balance approaches. The indirect methods do not disturb the plant canopy; however, they require large homogeneous fields to obtain stable and valid results.

ET measurement in green roofs is a recent issue in the academic community, which have used mainly indirect approaches and models (see Table 3) to simulate the real (RET) and potential evapotranspiration (PET) and to derive the components of hydro-thermal balance in the layers of the roof. For example, the Hargreaves or Penman-Monteith models were particularly used to estimate PET or the reference evapotranspiration (ET_o) (Marasco et al., 2015). In addition, many green roof models have been developed for the calculation of ET. They typically contain a dynamic thermal balance applied to each component of the green roof (support, soil and vegetated canopy) and compute the coupled mass heat transfer between them (Malys et al., 2014).

Table 3. Methodologies used to measure evapotranspiration in a green roof.

Reference	*Description*	*Formula*
Measure of ET by water balance		
Wadzuk et al., 2013	Water balance.	ET is measured using a water balance from a weighing lysimeter. $$ET = P + Ir - Qr - \Delta\theta z_s$$ The change in moisture content over the soil depth is quantified as the change in lysimeter weight.
Berretta et al., 2014	SMEF Model (Soil Moisture Extraction Function). *Estimated the ET under conditions of restricted moisture availability.*	ET at a generic time t is a function of potential evapotranspiration PET_t at the time *t* multiplied by the ratio of actual moisture content (θ_t) to the moisture content at field capacity (θ_{FC}). $$ET_t = PET_t \cdot \frac{\theta_t}{\theta_{FC}}$$
Poë et al., 2015	Experimental set-up to monitoring mass balances changes.	ET is inferred as changes in the moisture (θ) from both vegetated and non-vegetated configurations of each microcosm. $$ET = \frac{\theta_t}{\theta_{MAX}} \times PTE$$ Microcosms consist in nine different green roof configurations, comprising combinations of three substrates and three vegetation treatments.
Tan et al., 2017	ET rates per minute determined by mass balance. *ET inferred as changes in the mass of planter box: measured by*	ET rate is function of the mass (M) variation in the box planted in one day and the area of the plot (A_{plot}). $$ET_d = \frac{M_{d+1} - M_d}{A_{plot}}$$ There are three configurations of planted box

Reference	Description	Formula
	weighing the middle planter box.	with variation of the substrate type and the presence or absence of the water retention layer.
Measure of ET by latent heat flux		
De Munck et al., 2013	ISBA Model (Interaction between Soil Biosphere and Atmosphere). *Estimated the plant transpiration through surface flux et latent heat.*	Latent heat flux (Qe), is the sum of the plant transpiration (Qe_{TR}), the soil vegetation (Qe_g), and the evaporation of the water intercepted by plant foliage (Qe_r): $$Qe = Qe_{TR} + Qe_g + Qe_r$$ Fluxes estimated by detailed parameterizations, especially Qe_{TR}, based on the fraction of vegetation covering the ground (F_{veg}); the air density (ρ_a); the turbulent exchange coefficient (C_H); the wind speed (U_2); the Halstead coefficient (H_v) and the vapour pressure deficit in the air (VPD): $$Qe_{TR} = F_{veg}\rho_a C_H U_2 H_v (VPD)$$
Barrio, 1998	Based in the Newton Law of convection. *Measuring of the transpiration flux.*	The energy flux consumed to let water evaporate in leaves may be represented by a law analogous to the Newton Law convection: $$Qe_{TR} = -2LAI\frac{\rho C_p}{\gamma(r_e + r_i)}(e_p - e_a)$$ The latent flux of the plant depend of the Leaf area index *(LAI),* the thermodynamic psychometric constant *(γ)*, the vapor pressure at the leaf surface *(e_p)* and at the canopy air *(e_a)*. Also influences the canopy external resistance (r_e) to sensible heat transfer, the internal resistance (r_i) and the leaves specific thermal capacity (ρC_p).
Measure of ET flux by a dynamic chamber		
Marasco et al., 2015	*ET obtained from the variation of water vapor concentration flux (absolute humidity).*	The ET is obtained from water vapor at the start instant of measure ($w_c(0)$), and the saturation concentration of water vapor *(w_s)*, as well as the environmental initial conditions (pressure P_0 and temperature T_0). $$ET = \frac{P_0}{RT_0}\frac{1}{\left(1 - \frac{w_c(0)}{1000}\right)}k\left(\frac{w_s - w_c(0)}{1000}\right)$$
Ramier et al., 2015		The ET flux is a direct function of the variation in the time of the absolute humidity (ρv). $$Qe = 10^{-3}\lambda h\frac{\Delta \rho v}{\Delta t}$$

Reference	*Description*	*Formula*
Measure of ET flux based in modeling Penman-Monteith equation recommended by the FAO		
Malys et al., 2014	Taking into account a number of parameters and physical phenomena (radiation, sensible heat into the soil, the air temperature T, the saturated vapor pressure e_s, wind speed U_2, etc.) and characteristics of the plant.	Equation implemented in SOLENE model. $ET = \frac{R_n\Delta + \rho_a C_p \frac{e_s - e_a}{r_a}}{\lambda\left(\Delta + \gamma\left(1 + \frac{r_s}{r_a}\right)\right)}$ Do not take into account: - Soil moisture status - Type of vegetation
Ouldboukhitine et al., 2011		$ET = \frac{0.408\Delta(R_n - G) + \gamma\frac{900}{T_a + 273}U_2(e_s - e_a)}{\Delta + \gamma(T + 0.34U_2)}$

The main differences between models are: the calculation of the evapotranspiration rate, the canopy and substrate spatial discretization, and the moisture representation inside the substrate.

5. MATERIAL AND METHODS

5.1. Measurements of water content and temperature by TDR sensors

Soil moisture and temperature are important variables controlling the exchange of water and heat energy between the land surface and the atmosphere. Soil moisture particularly helps to determine the proportion of rainfall divided into runoff, surface storage and ET, as well as the proportion of the net radiation balance split into latent, sensible and soil heat flux (Jackson et al., 2008; Lakshmi et al., 2003). By looking at the water balance equation in dry periods (P, Ir and Qr are assumed to be zero), ET is directly related to the water storage variation into the soil, which is determined by the average moisture content as follows:

$$\Delta S = \Delta\theta z_s \tag{5}$$

Where $\Delta\theta$ is the average moisture content [m^3/m^3], z_s is the depth of the soil [mm].

Consequently, the relationship between soil moisture and evapotranspiration is given by the following equation:

$$ET = -\Delta S = -\frac{\Delta\theta}{\Delta t} z_s \tag{6}$$

Where Δt is the time step of analysis.

Observations and estimations of surface temperature and soil moisture are difficult to perform, as both are spatially (as a function of soil type, depth or porosity) and temporally variable (Lakshmi et al., 2003). Hence, adequate systems are required to properly assess the soil moisture. Today a large number of sensors based on different methods are available for measuring soil moisture (Jackson et al., 2008). Indirect methods based on electromagnetic (EM) principles have gained wide acceptance over the last decades because they can deliver, fast, operational, in-situ, non-destructive and reliable measurements with acceptable precision (Stacheder et al., 2009).

Here Time Domain Reflectometry technique (TDR also known as capacitance) has been selected. It is an electromagnetic moisture measurements that determines an electrical property called electrical conductivity or dielectric constant (k_a). It is based on the interaction of an electromagnetic field and the water by using capacitance/frequency domain technology

Measurement Principle

The TDR sensor measures the propagation time of an EM pulse, generated by a pulse generator and containing a broad range of different measurement frequencies. The electrical pulse is applied to the waveguides (traditionally a pair of parallel metallic rods) inserted into the soil. The incident EM travels across the length of the waveguides and then is reflected back when it reaches the end of the waveguides. The travel time required for the pulse to reach the end of the waveguides and back depends on the dielectric constant of the soil.

$$k_a = \left(\frac{c \cdot \Delta t}{2 \cdot L}\right) \tag{7}$$

Where L the effective probe length, Δt is the two-way travel time along the probe, and c the velocity of EM wave in free space (c=2.298×10^8 m/s)

Then it is possible to estimate soil moisture content by analyzing the dielectric constant changes into the soil. The usual relationship between volumetric water content and dielectric constant is known as Topp's Equation (Topp et al., 1980). It is adapted to a homogeneous mineral soil:

$$\theta = -5.3 \times 10^{-2} + 2.92 \times 10^{-3} k_a - 5.5 \times 10^{-4} {k_a}^2 + 4.3 \times 10^{-6} {k_a}^3 \quad (8)$$

Where θ is the volumetric soil water content [$m^3.m^{-3}$] and k_a the bulk soil dielectric permittivity [-]

Consequently, a ubiquitous wireless TDR sensor network has been implemented on the ENPC Green Wave to measure both water content and temperature. For this purpose thirty-two CWS665 wireless TDR sensors (produced by Campbell Scientific ®) have been installed on the BGW. Dielectric constant, volumetric water content and bulk electrical conductivity are derived from these raw values. The data are collected by some CWB100 wireless bases, able to store the data of eight sensors. Then data is transferred to a data-logger CR6 from Campbell Scientific (see Figure 5). These 32 sensors aim to capture the space-time variability of water content in a heterogeneous soil as the GW substrate. They are particularly adapted to assess the influence of the slope on infiltration and evapotranspiration processes.

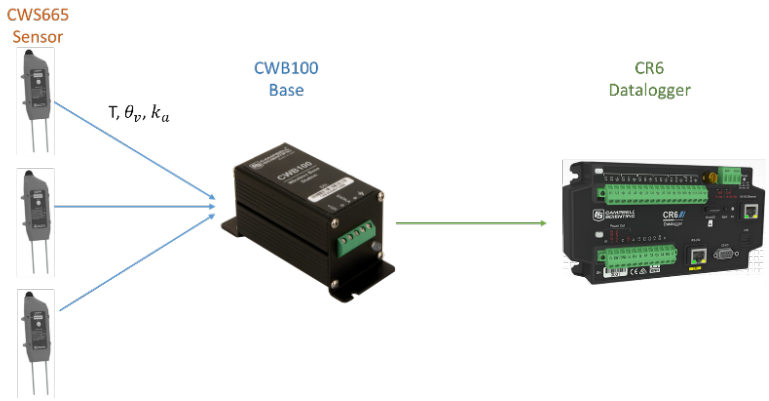

Figure 5. Soil moisture and temperature measurement

5.2. Dynamic transpiration chamber

The dynamic transpiration chamber represents a direct method to measure ET. It includes some equipment to assess and isolate gas samples from plant canopies (Luo et al., 2018), and analyze the changes of water vapor and carbon dioxide concentrations. Dynamic transpiration chamber measures the variation of water vapor exchange (vapor density) between the soil surface and the atmosphere, while this one is placed on a small (cm^2) or medium (m^2) section of surface (Garcia et al., 2003; Marasco et al., 2015).

The use of chambers for ET measurements has been criticized on the basis that the net radiation and microclimate within the chamber may not be representative outside the chamber, but different studies have proved that the portable chamber could provide a reasonable measure of ET with result in close agreement to other methods (McLeod et al., 2004).

Measuring Principe

Once the chamber is installed on the vegetation or on the ground, it is possible to record the increase of vapor density during a certain period of time, thanks to gas analyzers. It is

assumed that within this short measurement period, there is no microclimate change inside the chamber and that saturation vapor pressure is not reached. The variation of vapor density (Figure 6) is assumed to be proportional to the ET flux from the surface area enclosed by the chamber (Loustau et al., 1991; McLeod et al., 2004; Stannard, 1988).

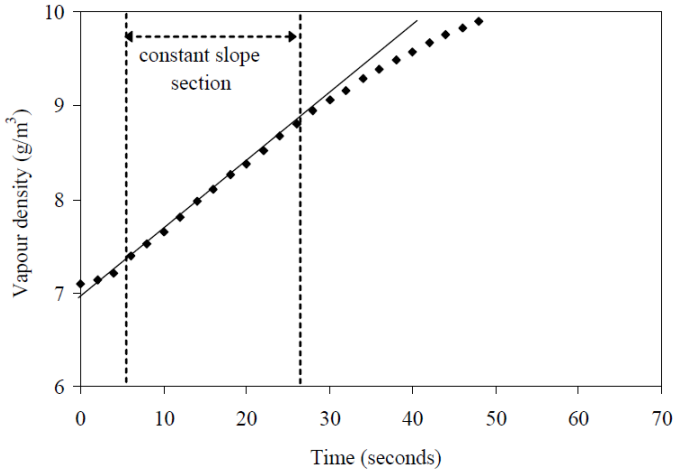

Figure 6. Vapor density in the ET chamber, (McLeod et al., 2004)

Vapor density measurement is usually carried out for a period of 1 to 2 [min]. They stop before the ET produced from plants start to decrease due to the increased vapor or CO_2 concentration within the chamber. Small rotating fans with variable speed are used to mix the air and water vapor within the chamber thus ensuring that the air under the chamber was representative of outdoor conditions by the single temperature and humidity sensors. Measurements can be repeated at various times in several locations (McLeod et al., 2004).

ET rate at a single location for one measurement is computed from the constant-slope section of the vapor-density time series. Few factors contribute to the lack of immediate establishment of the constant slope after the start time. This transient period can last from approximately 5 to 15 [s]. The constant-slope section persists until increased vapor-density concentration begins to decrease ET (Stannard, 1988).

The ET chamber used for this study corresponds to that build at Cerema (*Centre D'études Et D'expertise Sur Les Risques, L'environnement, La Mobilité Et L'aménagement*). This chamber consists of a Plexiglas compound enclosed (Figure 7) with an area of 1 m^2 and a height of 30 cm. The metal base makes it possible to seal the chamber with the floor (Ramier et al., 2015). It contains:

- an absolute humidity sensor [g /m^{-3}]: Gaz analyser LI-7500 from LI-COR
- a temperature sensor (°C): T107
- a net radiation sensor: Radiometer NR-Lite from Kipp&Zonen

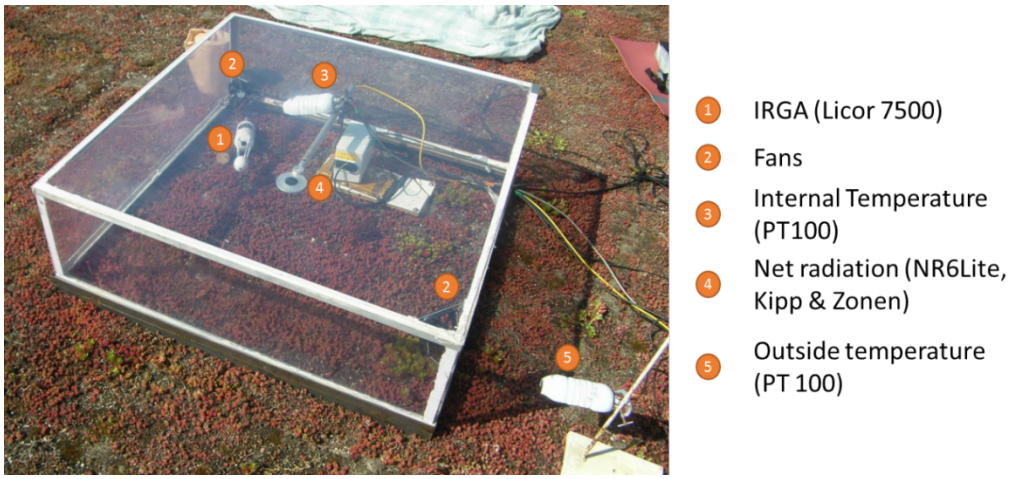

Figure 7. Evapotranspiration chamber, (Ramier et al., 2015)

The relationship between ET and the absolute humidity variation over this period of time is presented as follows (Ramier et al., 2015):

$$Qe = 10^{-3}\lambda h\frac{\Delta \rho v}{\Delta t} \quad (9)$$

Where Qe is the evapotranspiration flux [W m^{-2}], λ is the latent heat of vaporization of water [J kg^{-1}], h is the height of the chamber [m], ρv is the absolute humidity [g m^{-3}] and t is the time [s]. The absolute humidity variation $\frac{\Delta \rho v}{\Delta t}$ is calculated through a linear regression during the first minute of measurement.

5.3. Scintillometer and energy budget

Optical scintillation methods have been recognized by various authors (Guyot et al., 2009; Moene, 2003; Moorhead et al., 2017; Valayamkunnath et al., 2018; Yee et al., 2015) as an accurate suitable tool to estimate atmospheric surface fluxes, such as the sensible heat flux and to indirectly derive ET through the energy budget equation over a large heterogeneous and complex area.

A scintillometer is an instrument that consists of a transmitter that emits electromagnetic (EM) wave signal to a receiver, which record the turbulent intensity of this signal from a horizontal path length (Yee et al., 2015). When EM radiation propagates through the atmosphere, it is distorted by a number of processes that can influence its characteristics, e.g., its intensity. Two of these processes are scattering and absorption by constituent gases and atmospherics particles of the atmosphere, which remove energy from the beam and this leads to attenuation (Meijninger et al., 2002). The most serious mechanism that influences the propagation of EM radiation is small fluctuations on the refractive index of air (n). The signal is scattered by turbulent eddies in the atmosphere and detected as fluctuations in the intensity recorded by the scintillometer, known as scintillations (Moene, 2003; Yee et al., 2015).

The land surface acts as a transitional layer between the boundary layer and the subsurface soil column, regulating land-atmospheric interaction processes through the transfer of energy and water (Valayamkunnath et al., 2018). Thus, the thermodynamic structure of the surface layer is impacted by the turbulent heat fluxes (Q_h and Q_e), major drivers of atmospheric circulation.

Optical Large Aperture Scintillometer (LAS)

The most commonly used scintillometer for sensible heat measurement is the large-aperture scintillometer (LAS) (Valayamkunnath et al., 2018), since it operates in the invisible and near-infrared wavelength region, where the scintillometer is primarily sensitive to temperature fluctuations (Meijninger et al., 2002). The main components of LAS include a transmitter to emit an near-infrared beam (880 nm) at the focus of a concave parabolic mirror and a receiver to measure the fluctuations of the beam *(*Figure 8*)* that are caused by the properties of the air such as the turbulence, induced atmospheric scintillation (Valayamkunnath et al., 2018).

This turbulence phenomena corresponds to the behavior of flows in the atmospheric boundary layer (ABL). Turbulence consists of a wide range of three-dimensional whorls, usually called eddies, and generated by both wind shear and convection, and have a size in the order of magnitude of the boundary layer depth. The variance of the received signal is related to the refractive index structure parameter C_n^2, which is related to the fluctuation of thermodynamic parameters, mainly air temperature and humidity (water vapor content) along the path between a transmitter and a receiver, induced by turbulent eddies (Guyot et al., 2009; Moene, 2003).

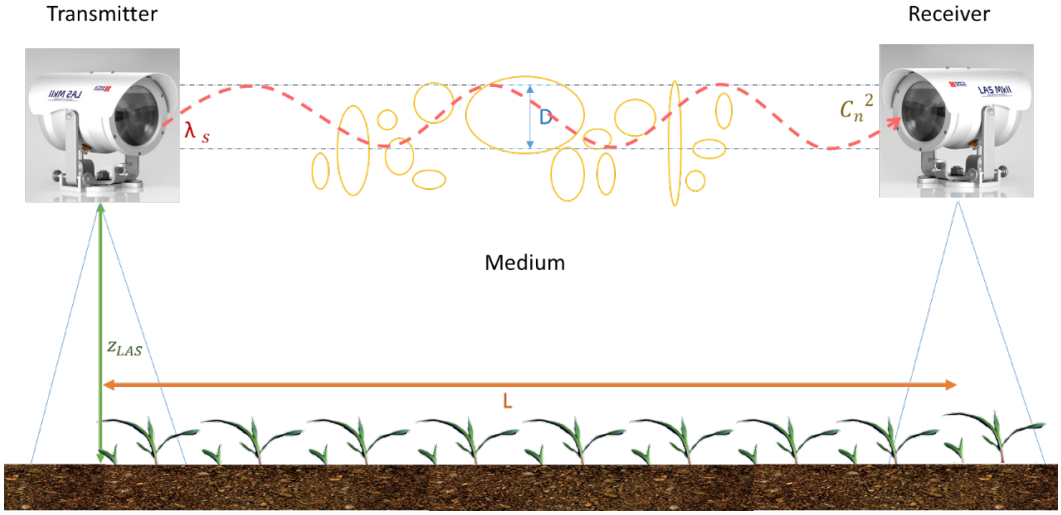

Figure 8. LAS Scintillometer implementation

Measurement Principe

The recorded fluctuations (scintillations) can be used to calculate the structure parameters for temperature and humidity, and sensible heat. An average sensible heat flux (Q_h) over path length of up to several km can be derived from infra-red (LAS) measurements (Guyot et al., 2009; Lagouarde, 2000). The device uses in this study is a produced by Kipp & Zonnen (Kipp & Zonen B.V., 2015).

LAS measures the fluctuation intensity logarithm variance (σ_x^2) of the EM signal (scintillations), a measure of the turbulent behavior of the atmosphere and it can indirectly be related to the transport of certain quantities. Depending on the configuration of the scintillometer (e.g. the aperture size, wavelength and the number of receivers), the fluxes of heat, water vapor and momentum can be derived (Meijninger et al., 2002).

For the LAS, the relation between the propagation statistics of the electromagnetic radiation (σ_x^2) and the atmospheric averaged structure parameter of the refractive index of air (C_n^2), is as follows (Wang et al., 1978):

$$C_n^2 = 1.12\sigma_x^2 D^{7/3} L^{-3} \tag{10}$$

Where, L is the distance between the transmitter and the receiver (i.e., the path-length) and D the aperture diameter of the transmitter and receiver.

The fluctuation of the refractive index of air depends on the composition of the gas and its state variables: pressure, humidity and temperature. The structure parameter C_n^2 is a function of the temperature (T) and to a lesser degree of the humidity (Q), hence C_n^2 can be decomposed as follows (Hill et al., 1980):

$$C_n^2 = \frac{A_T^2}{\bar{T}^2} C_T^2 + \frac{2A_T A_Q}{\bar{T}\bar{Q}} C_{TQ} + \frac{A_Q^2}{\bar{Q}^2} C_Q^2 \tag{11}$$

Where A_T and A_Q are functions of the beam wavelength, the mean value of temperature, humidity content, and the atmospheric pressure. In the visible and near-infrared wavelength region of the EM spectrum, A_T and A_Q are defined as follows:

$$A_T = -m_1(\lambda)\left(\frac{P}{T}\right) - R_v m_2(\lambda)\, Q \qquad A_Q = R_v m_2(\lambda) Q \tag{12}$$

In case of infrared wavelength: $m_1(\lambda) = 0.78 \cdot 10^{-6}\ [\mathrm{K\,Pa^{-1}}]$, $m_2(\lambda) = -0.126 \cdot 10^{-6}\ [\mathrm{K\,Pa^{-1}}]$, and R_v is the specific gas constant for water vapor $461.5\ [\mathrm{J\,K^{-1}\,kg^{-1}}]$:

$$A_T = -0.78 \cdot 10^{-6}\left(\frac{P}{T}\right) + 0.126 \cdot 10^{-6} R_v Q \qquad A_Q = -0.126 \cdot 10^{-6} R_v Q \tag{13}$$

Typical values of A_T and A_Q for normal atmospheric conditions are $-0.27 \cdot 10^{-3}$ and $0.70 \cdot 10^{-6}$ respectively. As an optical scintillometer is more sensible to variations of temperature than humidity, and A_T is much larger than A_Q (Kipp & Zonen, 2015). Hence, for near infrared signals C_n^2 can be expressed by a direct function of the temperature structure parameter C_T^2 (Guyot et al., 2009), simplifying the Equation 10 (Wesley, 7960):

$$C_n^2 \approx \frac{A_T^2}{T^2} C_T^2 \left(1 + \frac{0.03}{\beta}\right)^2 \quad \text{or} \quad C_n^2 \approx \left(\frac{-0.78 \cdot 10^{-6} P}{T^2}\right)^2 C_T^2 \left(1 + \frac{0.03}{\beta}\right)^2 \tag{14}$$

Where, β is the Bowen ratio, which is defined as the ratio between the turbulent heat fluxes ($\beta = Q_h/Q_e$). This term is a correction for humidity fluctuations (scintillations). Moene (2003) has shown that this correction is not necessary in most situations because for large β values, the correction is insignificant, whereas for small (i.e. for weak sensible heat fluxes) the absolute correction on Q_h remains small with respect to the other energy fluxes. Thus, when the surface conditions are dry, C_T^2 is directly proportional to C_n^2:

$$C_n^2 \approx \frac{A_T^2}{T^2} C_T^2 \quad \text{or} \quad C_n^2 \approx \left(\frac{-0.78 \cdot 10^{-6} P}{T^2}\right)^2 C_T^2 \tag{15}$$

Once C_T^2 and C_n^2 are known, jointly with the air temperature, wind speed and air pressure, it is possible to determine the fluxes of heat and water vapor (Meijninger et al., 2002). The area-average sensible flux Q_h estimated from a LAS are based on the *Monin-Obukhov Similarity Theory (MOST),* which establishes a relationship between Q_h and C_T^2 (Moene, 2003).

MOST is applied to the lowest layer of the Planetary Boundary Layer (PBL), denominated the Surface Layer (SL). Within the SL, it is considered that the vertical fluxes of momentum and conservative scalars are nearly constant with height. Assuming stationary conditions and a horizontal homogeneous surface, MOST describes this relationship as follows:

$$\frac{C_T^{\,2}(z_{LAS}-d)^{2/3}}{T_*^{\,2}} = f_T\left(\frac{z_{LAS}-d}{L_{MO}}\right)(L_{MO}<0) \tag{16}$$

Where, d is the zero-displacement height (height at which the mean velocity is zero due to large obstacles such as buildings/canopy), z_{LAS} is the effective height of the scintillometer beam above the surface, f_T is the universal function of the stability parameter $z_{LAS}-d/L_{MO}$, while L_{MO} is the Obukhov length and T_* is the MOST temperature scaled (Kipp & Zonnen-Manual). Temperature scaled integrates Q_h and a parameter of friction velocity u_*.

Table 4. Main equations conducting the MOST theory

T_* inversely proportional to L_{MO}	u_* is estimated using the stability function Ψ (z/L_{MO}) given by Panofsky and Dutton (1984)	Q_h can be derived from a iteratively process
$T_* = \frac{u_*^{\,2}T}{gk_vL_{MO}}$ (17)	$u_* = \frac{k_v u}{\ln\left(\frac{z_u-d}{z_0}\right)-\Psi\left(\frac{z_u-d}{L_{MO}}\right)+\Psi\left(\frac{z_0}{L_{MO}}\right)}$ (18)	$Q_h = \rho_a C_p u_* T_*$ (19)
Where g is gravitational acceleration, k_v is the Von Karman constant, z_0 is the roughness length (height at which the main velocity is zero due to the substrate roughness), z_u is the height at which the wind speed is measured, Ψ correspond to the stability correction function for momentum transfer and C_p is the specific heat of the air at constant pressure ($-1005\ \mathrm{J\,kg^{-1}\,K^{-1}}$).		

Sensible heat flux is derived from Equation (19, through iterations on L_{MO}, T_* and u_* (using Equations 15, 16 and 17).

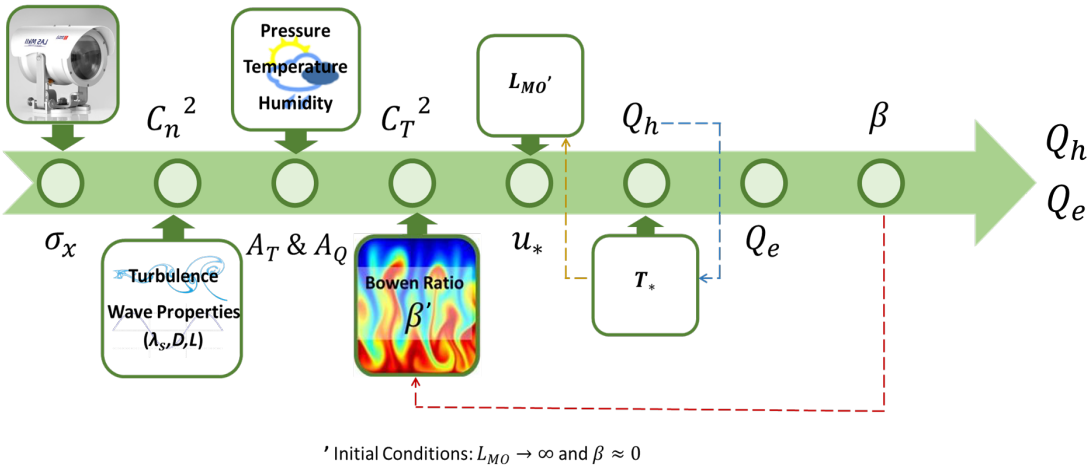

' Initial Conditions: $L_{MO} \to \infty$ and $\beta \approx 0$

Figure 9. Scintillometer measurement process.

Finally, the latent heat flux (Q_e) can be derived from the energy balance ($R_n = Q_g + Q_e + Q_h$ (2), the data of net radiometer and soil heat flux provided by sensors.

6. PRESENTATION OF THE RESULTS

6.1. Evapotranspiration flux from soil moisture content

As mentioned earlier, 32 wireless sensors are implemented on the GW. They measure temperature and the soil dielectric constant. These were initially installed as a grid, each 3 m horizontally (4) and vertically (8). The data was collected from two periods: February 05th to April 28th and September 27th to 30th. Dielectric constant data was transformed to volumetric soil water content (θ or VWC), through the Topp's Equation (Figure 10) for 16 active sensors located in the center of the grid. The maximum value of moisture content recorded on the BGW during the analysis period was 0.38 [m^3m^{-3}] and the minimum was 0.259 [m^3m^{-3}] between the February 05th to April 28th.

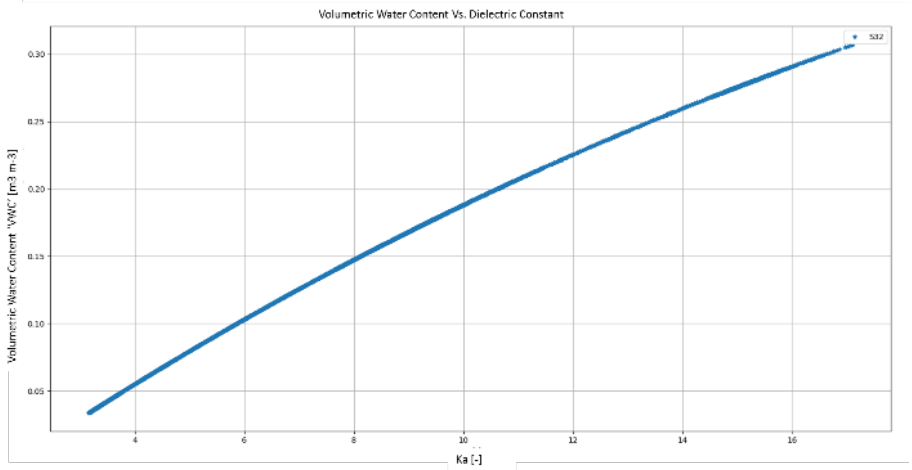

Figure 10. Volumetric Water Content Vs. Dielectric Constant.

The VWC variation was analyzed in parallel with the rainfall time series to determine the dry periods (without precipitation). The rainfall series was obtained from the data collected by three disdrometers located on the roof of the Carnot building at the Ecole des Ponts ParisTech campus. These disdrometers report rainfall intensity each 5 minutes.

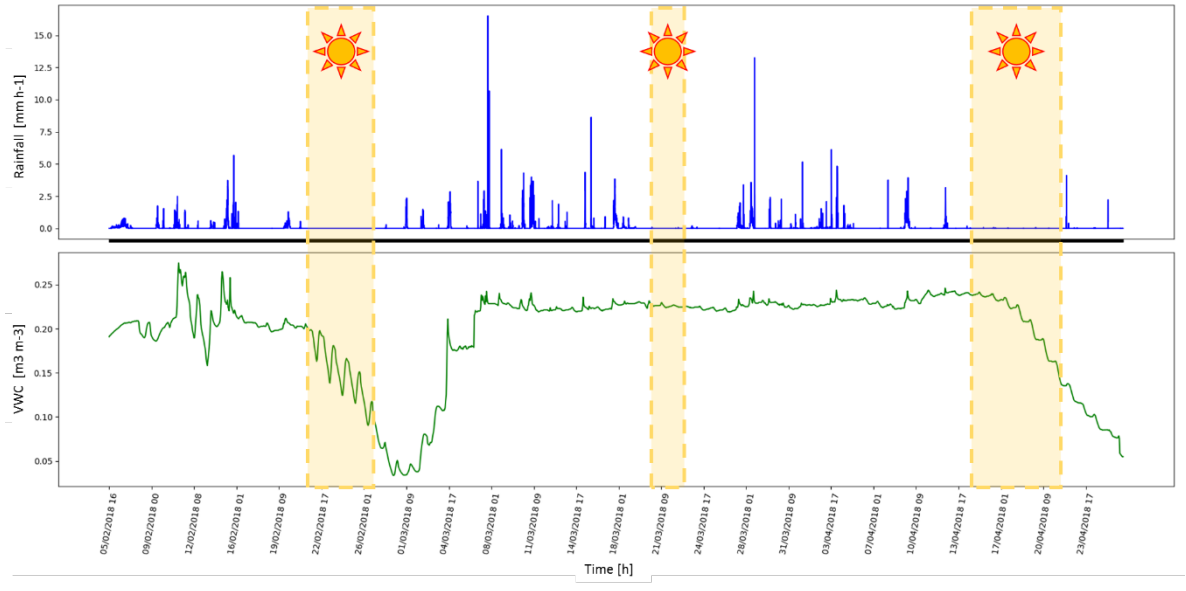

Figure 11. Temporal variation of VWC and Rainfall, and selection of 3 dry periods.

Three dry periods have been selected when there was no rain, irrigation and runoff, and also where there is an obvious decrease of soil water content (Figure 11): February 21st to 28th, March 20th to 22nd and April 13th to 17th. That allows to calculate directly the ET flux from the water balance and soil moisture content variations (Equation (6).

$$ET = -\Delta S = -\frac{\Delta \theta}{\Delta t} z_s$$

The dielectric constant recorded data was characterized by an important noise, which affected the computation of ET. This disturbance can come from precipitation (Luo et al., 2018) or the soil specific calibration (Guderle and Hildebrandt, 2015). In dry conditions, the resolution of the sensors can also be mentioned. A Savitzky-Golay smoothing filter was applied on the dataset to smooth the noisy signal. Savitzky-Golay filter performs a polynomial fitting to segments of data, using a low order polynomial with the method of lineal least squares and convolution of all the polynomials (Acharya et al., 2016). The convolution can be understood as a weighted moving average filter with weighting given as a polynomial of a certain degree (Chen et al., 2004). The coefficients of a Savitzky-Golay filter, when applied to a signal, perform a polynomial P of degree k, fitted to the signal measures, where N describes window size (Azami et al., 2012).

Two parameters must be determined to implement Savitzky-Golay filter: the degree of the smoothing polynomial (k) and the frame size (N). Generally, the best fit values of k and N are estimated using trial and error method (Acharya et al., 2016). For our k_α data, the best fit of k and N are 3 and 15, respectively.

Results for the dry periods of March and April confirm that the increase of soil temperature (related to climate conditions) is one of the principal factors that act upon the BGW to extract moisture content via ET (Berretta et al., 2014; Poë et al., 2015). The soil moisture content progressively decreases during the dry period, but it has daily fluctuations due to the daily air temperature variability.

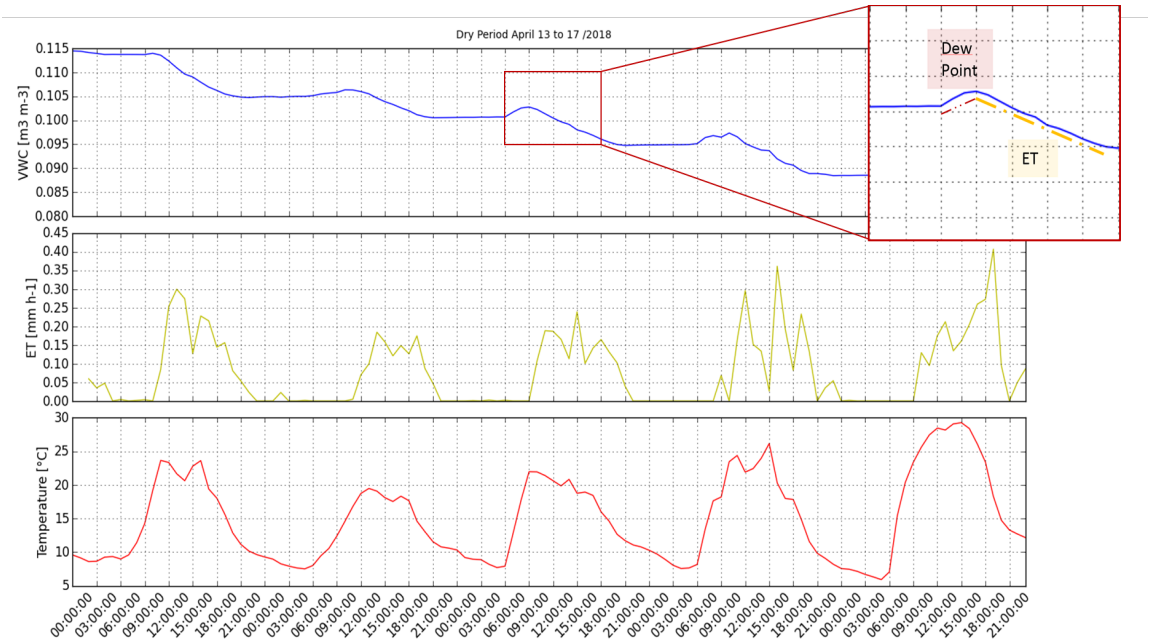

Figure 12. Evapotranspiration fluctuations during the dry period of April.

At the day scale, a general pattern can be proposed. During the night, VWC is constant because there is no phenomenon that forces the extraction of the water from the soil. However, it increases throughout the early hours of the morning (03:00 to 06:00h), when the lowest temperatures are recorded. This may be the consequence of air temperature over the vegetated layer reaching the dew point and producing the condensation of the water vapor. Once the soil volumetric water content reaches its maximum level and the temperature starts to increase, ET occurs during the day until the evening (Figure 12). It reaches its maximum level at noon and decreases during the afternoon. The maximum hourly ET rate is about 0.41 [mm h^{-1}] at 15:00, corresponding to the maximum recorded temperature value. ET values during April's dry period obtained from the moisture content variations are higher than those collected in March. This can be explained by higher temperatures, more solar energy and vegetation growth.

ET results obtained for February's dry period are different. First, moisture content is higher in winter conditions and the soil temperature values are lower, reaching -8 °C (Figure 13). During this season the sunrise occurs later, thus, the reaching of the dew point can provide water to the soil from the morning until noon, when the highest daily temperature is reached. At first, ET is generated once the temperature reaches its highest value (noon), until the sunset at 17:00h. This is associated to a common ET process driven by solar radiation. However, a second increment of ET is observed during the night despite the lack of irrigation, precipitation or runoff. This may be attributed to other atmospheric conditions that forced the ET at night, disturbing the water and energy budget of the structure. In this particular case, a greater wind speed at night was recorded in the closest meteorological station (Porte de Vincennes), reaching values of 11 km/h compared to April 3 km/h. According to Malek (1992), stronger wind speed increases ET at night because it facilitates the heat and mass exchange by means of convection from the soil to the atmosphere, leading to an increase of ET during the absence of daylight.

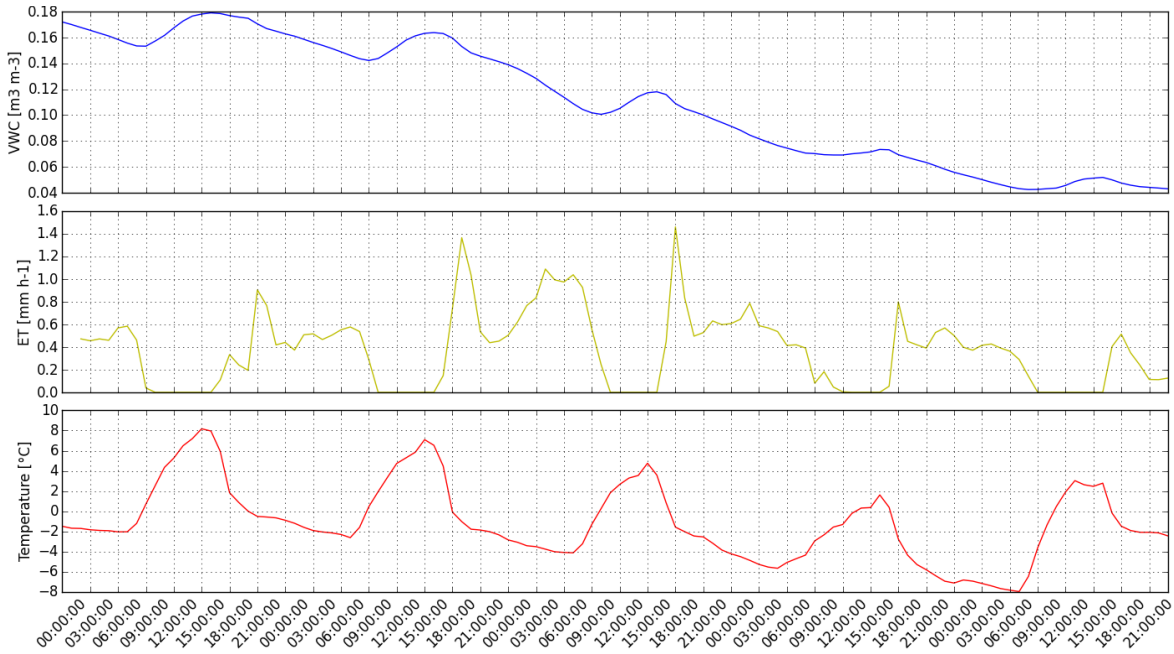

Figure 13. Evapotranspiration fluctuations during the February dry period.

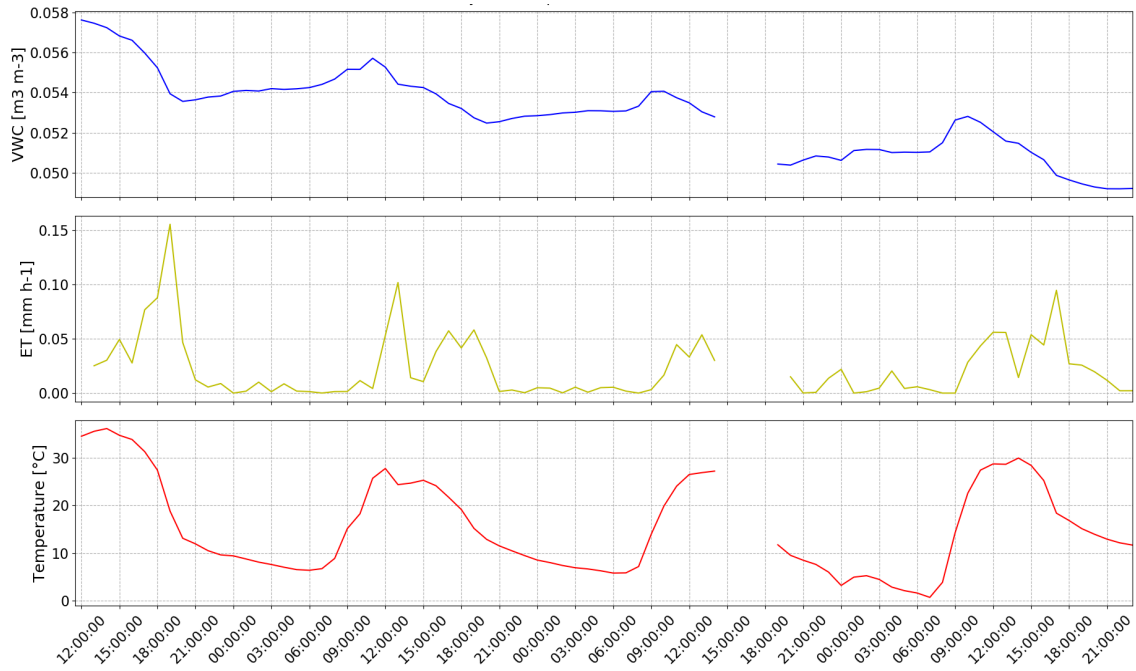

Figure 14. Evapotranspiration fluctuations during the September dry period.

Another analysis of ET computed from the water balance was made for a short dry period in September. The results obtained for this period are marked by lower water content in the soil, as result of the summer season with high temperatures and little rainfall. ET rate reached the maximum values of 0.15 [mm h^{-1}] at sunset, lower than those observed in April even though higher temperatures are recorded. ET rates in this period exhibited a reduction over time (Figure 14). According to Wadzuk et al., (2013) this behavior corresponds to the plants response to the higher water availability to support ET at the beginning of a dry period than one week after a rainfall event. Furthermore, little soil moisture variations at nighttime were recorded. In accordance with Caird et al. (2006), this behavior corresponds to the effect of transpiration of the plants, especially reported in warm and dry conditions.

ET measurements from water balance showed to be a good method to reflect the overall trends and dynamics of ET at the BGW. However, it has some disadvantages such as poor continuity, only can be calculate during long dry periods with high atmospheric demand (Guderle and Hildebrandt, 2015; Lakshmi et al., 2003; Schwärzel et al., 2009) and it has relatively low precision (Tie et al., 2018).

6.2. Evapotranspiration flux from dynamic transpiration chamber

The first two measurement campaigns with the transpiration chamber were carried out on 26th April and 1st June. During both experiments, the chamber was placed in three different locations of the BGW by considering its topography: the upper point correspond to the most elevated level of the wave (7 m over the ground), the middle point was placed in the intermediate level characterized by a significant slope, and finally the lowest point was placed at the lowest level of the wave, and was completely flat and close to the drainage area. The objective was to assess the possible influence of the BGW topography on the thermo-hydric processes. For the 26th April, 16 sensors of water content placed in their initial conditions/positions were used to compare the results with the chamber, while the 1st June the sensors were placed within the chamber (Figure 15).

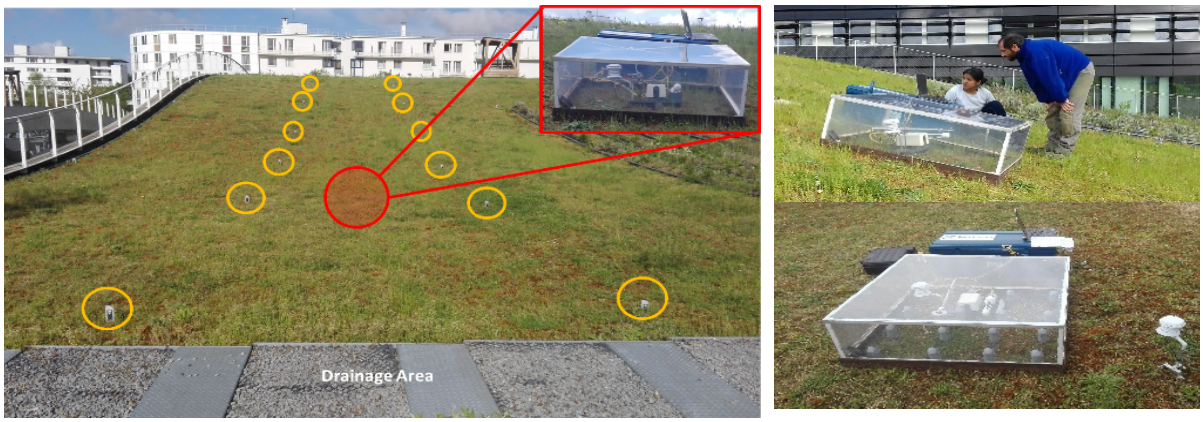

Figure 15. Measurements campaigns, a) and b) April 26 and c) June 1.

Latent heat flux (Q_e) was measured between 09:30 and 17:00. The results are highly variable for the three BGW locations for both measurement campaigns (Figure 16), but it is evident that Q_e tends to vary as a function of the net radiation which influences the air temperature. The absolute humidity (which is a direct function of the Q_e in Equation (9)) depends on the temperature and the water vapour pressure of the air. Consequently, the variations of the net radiation conditions influenced the flux of latent heat.

The meteorological conditions (rainfall > 5 [mm h^{-1}]) that occurred during the 1st June campaign prevented measurements between 11:30 and 14:00. However, it is possible to observe that after the rainfall event - that provides water to the soil -, and combined with the seasonal conditions of June (high temperatures), the flux of latent heat increases proportionally with the net radiation (Figure 16).

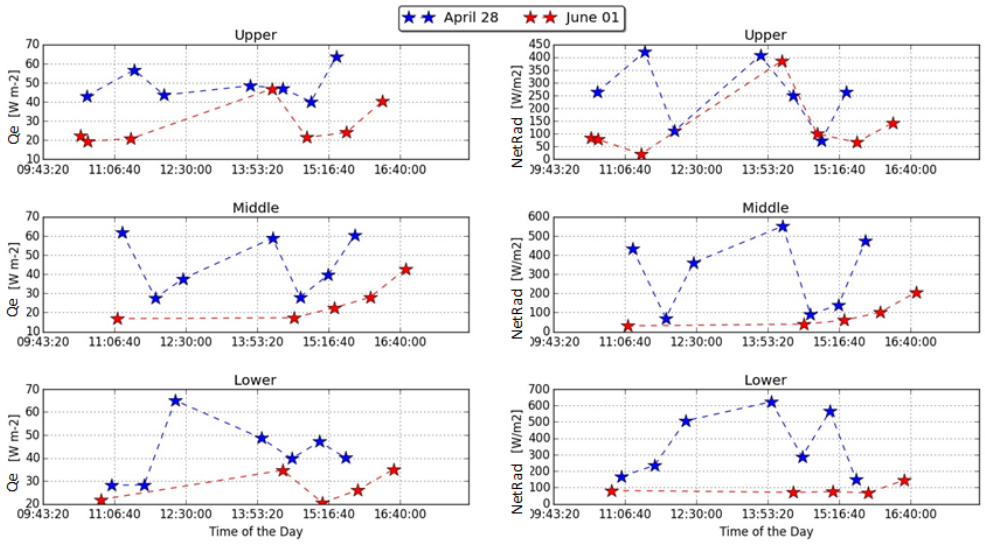

Figure 16. Latent heat flux and net radiation for three locations on the BGW.

Upper location shows the most stable measurements of Q_e over time, whereas the hourly measurements for the lowest point are clearly related to the net radiation, which increases at noon and reduces at sunset. However, there is no specific dynamic that differentiates or characterizes the latent heat flux in the three points of the roof by the transpiration chamber. Consequently to these results, the next measurements (20th June, 21st August and 26th and 27th September) were focused in the lower location, in order to stabilize the TDR measurements (which requires two hours minimum without displacements). The results show how the latent heat flux is more elevated (Figure 17) at the beginning of the summer season (20th June), forced by the increase of radiation flux, temperature, leaf growing rate and the availability of

water in the soil, due to the intense events of rainfall that occurred during the previous weeks (11th to 15th June).

Radiation impact over ET process is obvious thanks to the measurement carried out in August, during which the radiation rate was lower in comparison with the measurements done at the beginning of summer. According to the cloudy weather conditions, the latent heat flux rate was the lowest registered. Another element that affected the latent heat flux during this measurement is the restriction of water in the soil due to the drought-like conditions of this month.

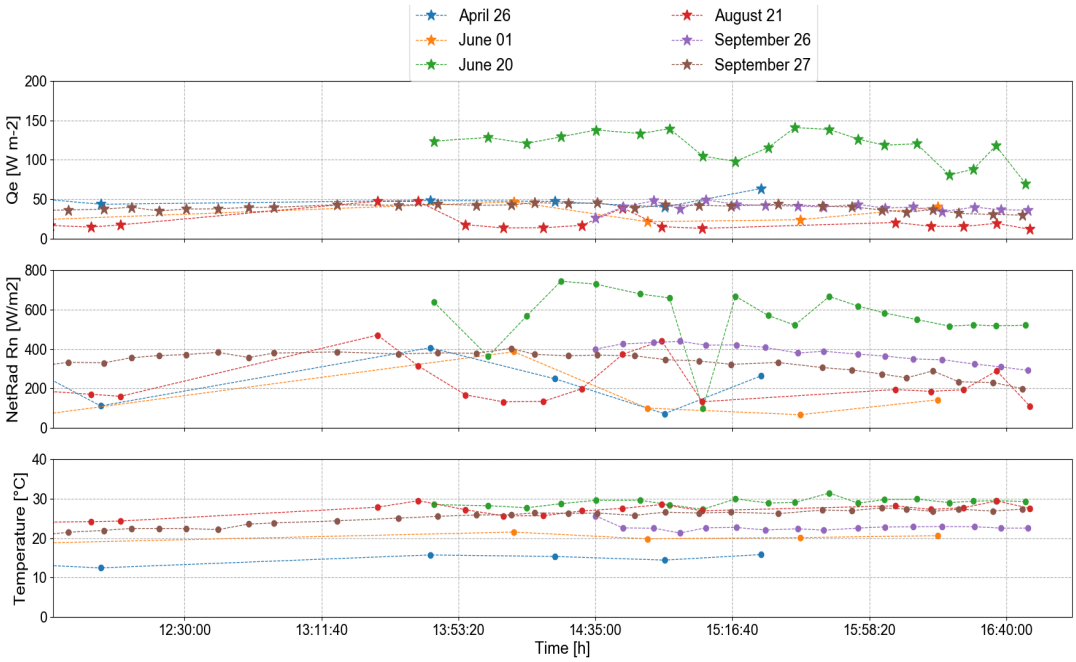

Figure 17. Latent heat flux, temperature and net radiation for the lower location of the BGW.

In general, the Q_e rates remains low on the BGW. In five of the six measurements made with the transpiration chamber, Q_e varies between 0.017 and 0.09 [mm h^{-1}], excepted in June 20th when the ET values reached 0.20 [mm h^{-1}] at 12:00 and 15:00, corresponding to the highest radiation recorded of 650 to 700 [W m^{-2}].

The data recollected in September 27th (Figure 18) allows to identify clearly the daily radiation variation during summer day and its effects over the Q_e flux variation, which achieves its maximum level at noon (12:00 to 14:00), when the solar energy or short wave radiation is at its maximum level, and decreases approaching zero toward the end of the day when the incoming short wave is negligible (McLeod et al., 2004).

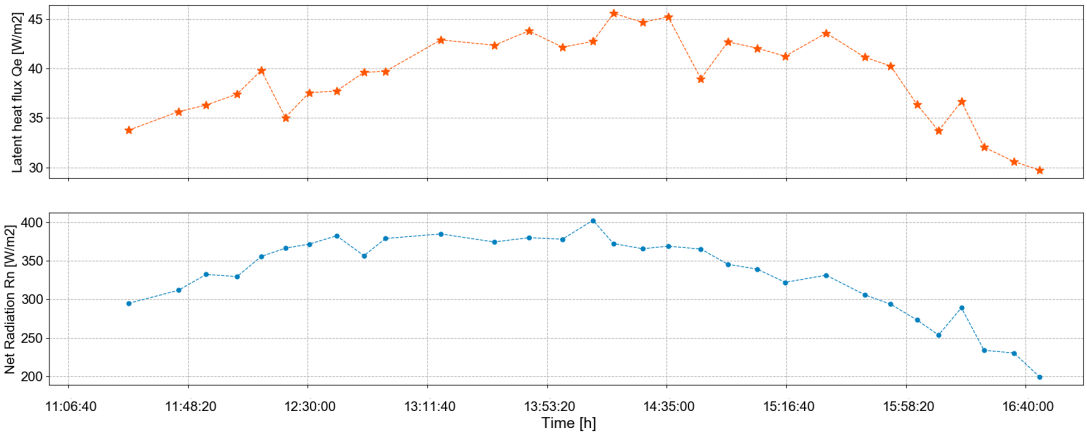

Figure 18. Transpiration Chamber Measurements, September 27th.

6.3. Comparison of ET deduced from the water balance and the transpiration chamber

Additionally, a comparison between the chamber and the sensors was carried out to analyse the ET estimated by both methods. For April 26th the closest sensor from the chamber was chosen for each location. In 1st June the sensors were displaced with the chamber in the tree locations of the BGW. For the next measurements in June 20th and September 27th, the chamber and 16 sensors were located in the lower point of the BGW without displacements, to insure the stability of the dielectric constant data.

In April 26th, the results obtained for the lowest point of the BGW (close to the drainage area), correspond to the highest levels of ET (Figure 19) computed from the water balance and the transpiration chamber: $\sim 0{,}65\ [mm\ h^{-1}]$ and $0{,}08\ [mm\ h^{-1}]$ respectively. This illustrates the availability of water near the drainage area, favouring the ET process (Marasco et al., 2015; Poë et al., 2015; Tan et al., 2017). These ET rates for April are consistent with other studies that measured similar soil moisture and ET values from the water balance: $0{,}0625\ [mm\ h^{-1}]$ during spring (Poë et al., 2015).

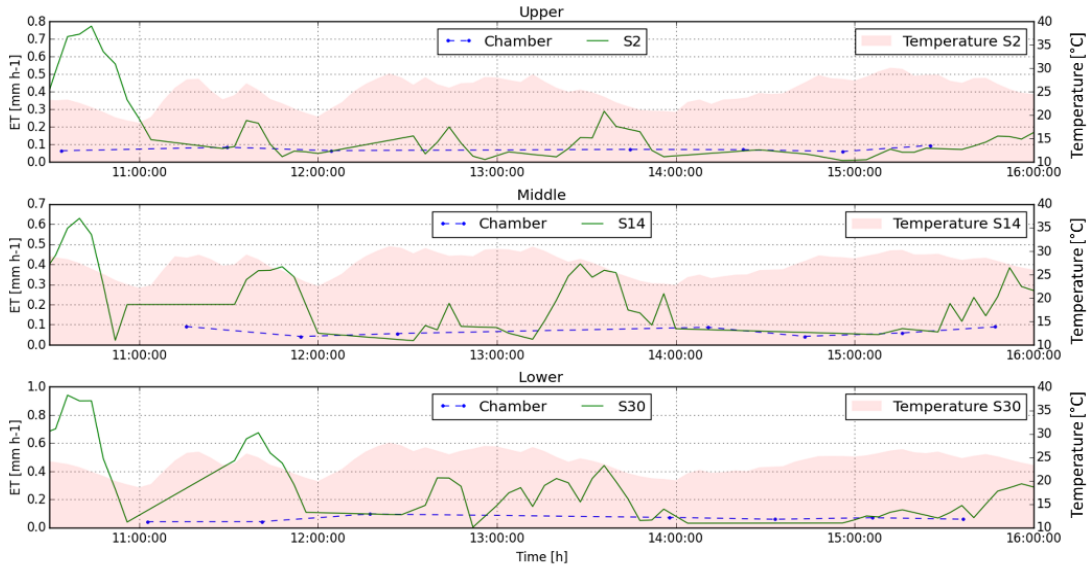

Figure 19. ET estimated from TDR sensors and transpiration chamber, April 26th.

In consequence of the rainfall event of June 1st and its consequences on the soil water content, the water balance method could be applied, because introducing significant errors in soil

water fluctuation (Fernández Gálvez et al., 2007), and finally the water loss by transpiration and evaporation (Schwärzel et al., 2009).

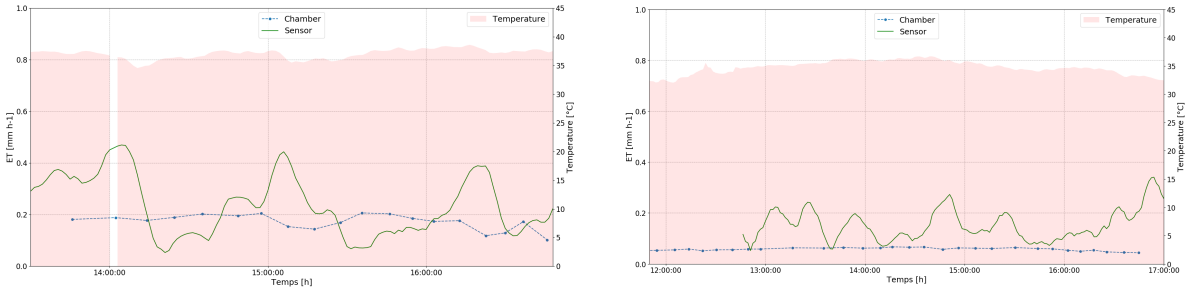

Figure 20. ET estimated from TDR sensors and transpiration chamber, June 20th (a) and September 27th(b).

By comparing the two methods on all experimental campaigns (Figure 19 and 20), it is shown that higher ET values are computed from the water balance, but without a clear daily pattern compared to the one estimated by the chamber. Some studies dedicated to ET estimation on extensive green roofs without irrigation and with vegetation type Sedum, have showed similar ET behavior than those measured on the BGW. Marasco et al., (2015) and Ramier et al., (2015), for example, reported ET rates of 0.2 $mm.h^{-1}$ in June, measured through a transpiration chamber. On the other hand, Wadzuk et al. (2013) reported average ET values obtained by water budget (measured with lysimeters) of 0.29 $mm.h^{-1}$ in September after a rain event and a temperature of 19 °C, while Marasco et al., (2015) measured ET rates of 0.04 $mm.h^{-1}$ in a green roof in New York, with temperatures ranging between 18 and 23[°C.

Some differences between the two methods (around 10%) have already been reported (Luo et al., 2018). One parameter that could conduct to this difference is the modification of the environmental conditions within the transpiration chamber, such as the radiation and the temperature. Another reason could be the characteristics of the soil where the sensors are implemented (Fernández Gálvez et al., 2007) and the horizontal water fluxes (i.e. hydraulic redistribution), which are not considered (Guderle and Hildebrandt, 2015), and can influence the water balance and lead to an overestimation of ET (Tie et al., 2018).

During this dry period, from August to September, the ET rate estimated from the chamber becomes lower than 0.07 [mm h^{-1}], while ET values deduced from the water balance was the lowest recorded 0.34 [mm h^{-1}]. This suggests that during summer, when the UHI intensity is stronger and the cooling effects of the green roofs are the most required, the ET process is lower than that occurring during the spring season. Some studies have already reported such response of green roofs, like a consequence of the low soil moisture availability (like was reported by the TDR sensors), necessary to support ET during summer (Cascone et al., 2018; Coutts et al., 2013; Marasco et al., 2015; Valayamkunnath et al., 2018).

6.4. Scintillometer measurements

Some tests and adjustment with the LAS scintillometer were carried out in a large hall and in an open space, before making measurements on the BGW. As result of these first experiments, various inconsistencies for an optimum measurement were detected, such as the elevated current adjustment in the transmitter and the low signal level in the receiver. This has an influence over the measurements of the structure parameter of the refractive index of air. In consequence, a review and possible update of the device was necessary from its manufacturer

(Kipp& Zonen) to use it adequately. However, a measurement campaign of two days was organized on the BGW (September 26th and 27th of September, from 10:30 to 17:00) to test this material in real conditions.

Scintillometer configuration was the same for the two days (see details in Table 5): the transmitter and the receiver were located on the highest point of the roof with a path length of 111.78 [m], and diaphragms for short range applications were placed in front of the LAS transmitter and receiver. During the two measurement campaigns, the weather was sunny, which facilitated the observation.

Table 5. LAS setting.

Path Length L [m]	111.78
Aperture Diameter of receiver and transmitter [m]	0.1
Height Transmitter [m]	1.37
Height Receiver [m]	1.04
Current Adjust knob [-]	1000
Path Length dial knob [-]	15.09
Signal Strength	≈ 45-50
Effective height LAS [m]	1.798
Roughness length (z_o)	0.25
Zero-Displacement height (d) [m]	1.75

During this campaign, a CNR4 radiometer (Kipp & Zonnen) was installed close to the LAS receiver to measure the radiative budget (Figure 21), and four K-Type thermocouples were implemented at different soil depths to estimate the soil heat flux. The CNR4 measures the balance between incoming and outgoing of both short and long-wave radiation. This equipment allow to estimate the net radiation used in the energy budget (Equation 2), as well as the surface albedo coefficient (α) of the BGW. The thermocouples were inserted vertically, close to the CNR4 radiometer and the LAS receiver. The distance between them was 1 to 2 cm, aiming to estimate the soil thermal gradient (Figure 22). The temperature and radiation data were stored in a Campbell Scientific CR3000 Data-logger with a sampling time of 10 minutes (like the scintillometer).

Figure 21. CNR4 Net Radiometer

Additional data is required to compute both latent and sensitive fluxes in the EVATION software, provided with the LAS. The meteorological data from the Paris-Orly station of Météo-France, corresponding to the air temperature and pressure, wind speed and direction, and humidity was also gathered for this purpose.

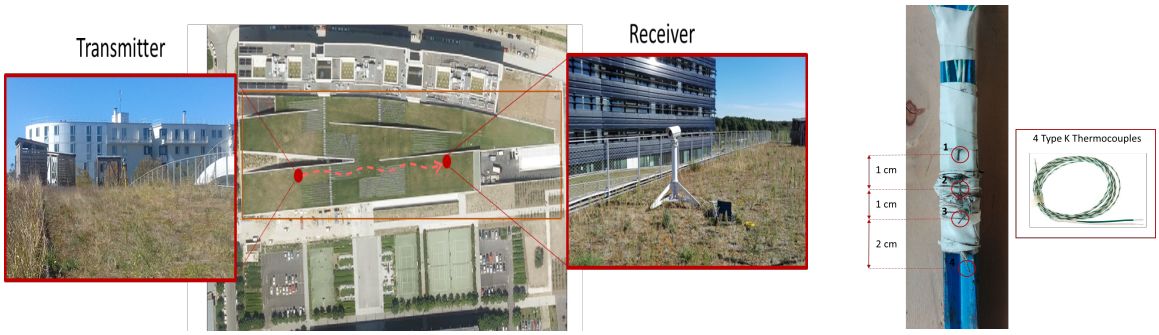

Figure 22. LAS Scintillometer localization on the BGW (left) and Type K thermocouples inserted in the soil (right).

Soil heat Flux:

Estimation of ground heat flux from the Fourier analysis using the harmonic model to calculate the soil temperature profile was not applied in this work, since the period of data collection was inferior to 24h (which is recommended) despite soil temperature varies according to the diurnal cycle (Cenis, 1989).

The data collected by the thermocouples placed in the deepest and superficial locations of the soil (z_1=2 and z_4=6 cm, respectively) were used to calculate the soil temperature gradient as a direct application of the Fourier Law (Equation 3). For this first approach with the LAS scintillometer, thermal conductivity (k) is assumed constant throughout the experiment and is based in the work carried out by Yang et al. (2018) in a green roof substrate characterized by a thickness and saturation of soil similar to conditions of the BGW (See section 4.3).

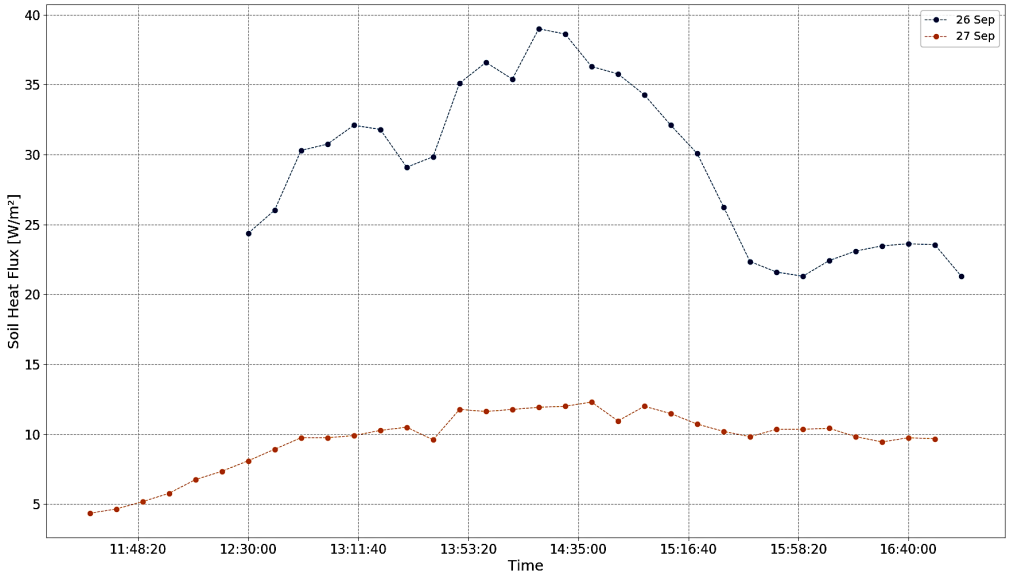

Figure 23. Soil heat flux BWG

The resulting conductive soil heat flux shown in Figure 23 exhibits two different curves. The first one corresponds to September 27th when Qg increases until noon and has a slight decrease until the end of the daylight, both driven by the solar radiation. The second one corresponds to September 26th, when Qg is higher due to a higher soil temperature, the main variable affecting the thermal gradient. The main reason of this difference is the conditions at which the thermocouples were implemented the first day of experiment (closer to the surface

and separated from two centimeters), leading to record higher temperatures and overestimate the soil heat flux in soil.

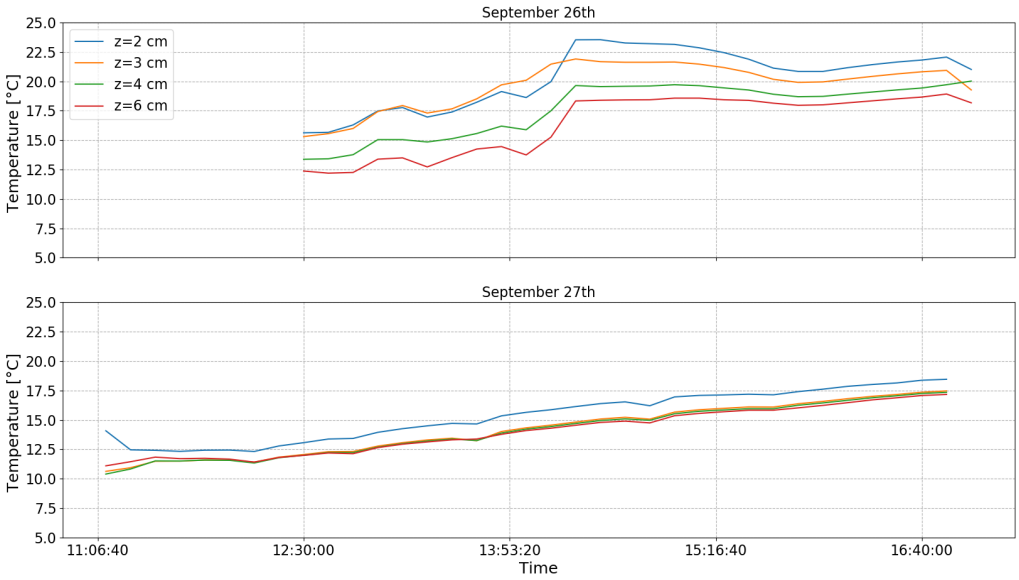

Figure 24. Soil Temperature Gradient

The effect of the thermocouples position on the soil heat estimation can be evidenced in Figure 24. There is a clear gradient of temperature achieving 5 °C for Sep 26th, while for Sep 27th the three thermocouples report similar values of temperature. Despite the differences of depth, only the thermocouple located close to the surface provides higher values. Moreover, on Sep 26th, the recorded data exhibits a peak of temperature at noon, and then a slight reduction in the afternoon, which matches with the daily radiation. On Sep 27th temperature remains constant on a large period of the day. This is particularly surprising as temperature is supposed to increase with the solar radiation and decrease during the night (see Cohard et al., 2018; Gagliano et al., 2016; Holmes et al., 2008 for examples). This irrelevancy should result from a poor contact between the thermocouples and the soil.

Surface fluxes:

To process the data and to estimate the surface fluxes based on the MOST (See section Scintillometer), the software from the LAS Scintillometer supplier 'EVATION' was used. The results of data processing contain the structure parameter of refractive index of air C_n^2, Bowen ratio β, albedo coefficient α and surface heat fluxes missing in the Equation 2 up to this moment (Latent heat Q_e and sensible heat Q_h flux). In practice the data were collected over unstable atmospheric conditions.

The different components of the energy budget estimated on the BGW from the LAS Scintillometer are presented in Figure 25. The energy budget closure is respected, when one component increases another decreases. The results suggest that R_n and Q_e are the most significant flux, R_n being the main energy input of the green roof.

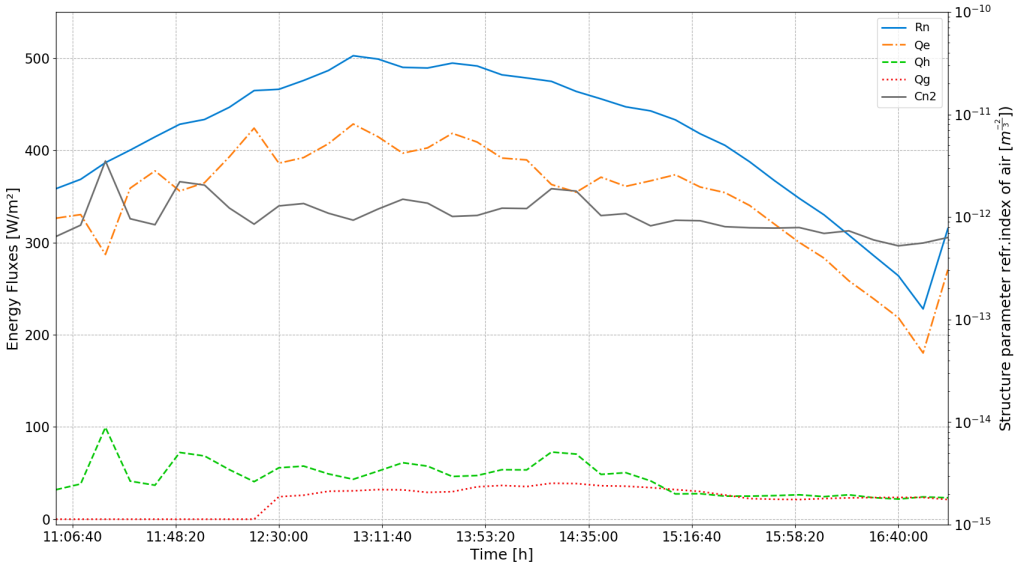

Figure 25. Energy fluxes on the BGW - September 26th

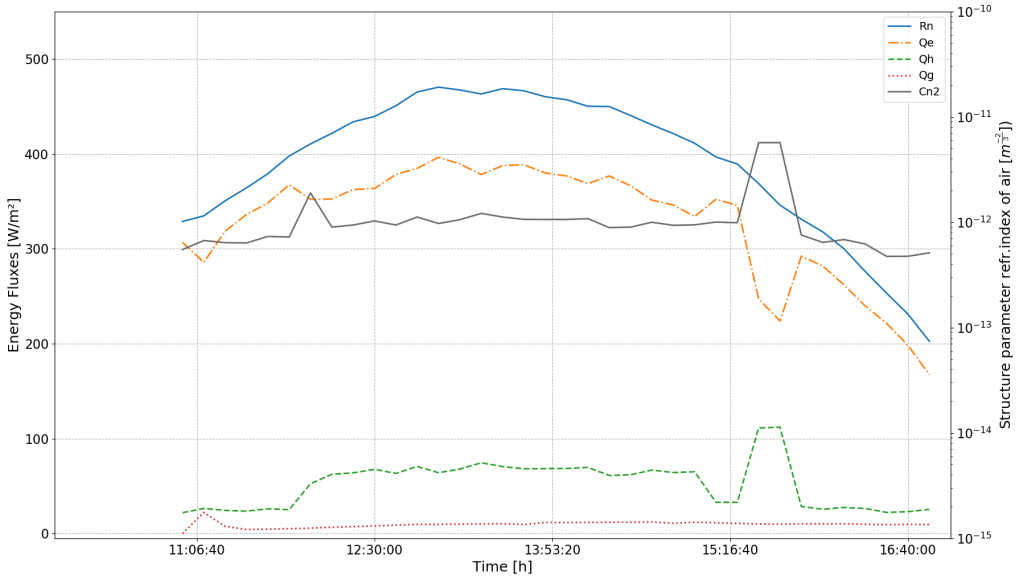

Figure 26. Energy fluxes on the BGW - September 27th.

The values of Q_h and Q_g fluxes are lower in comparison with Q_e, term deduced from the energy balance. Considering, the failures in the first mountings of the LAS, the low signal recorded at the receiver can lead problems in the estimation of C_n^2, and consequently, of β and Q_h too. Hence, one raison of the overestimation of Q_e can be the result of an underestimation of Q_h.

In addition to the low reception of the recorded signal, the transmitter and receiver were installed at 1.37 m and 1.04 m above the surface, respectively. However, the minimum height recommended by the manufacturer to non-violate MOST and to prevent the saturation phenomenon with the short-range diaphragms must be 1.5 m. This saturation zone is where the turbulence cannot be considered like horizontally homogeneous because is not in equilibrium with the local vertical gradients of structure parameter and the relationship between the amount of scintillations (σ_x^2) and C_n^2 is no more respected (Kipp & Zonen B.V.,

2015; Meijninger et al., 2002). Therefore, it is possible the LAS scintillometer was used inappropriately in the saturation zone.

Finally, ET from soil moisture content, transpiration chamber and LAS scintillometer measurements were compared in order to assess the relevance of the data collected in a single day (September 27th). Figure 27 shows the daily evolution of the ET through the three methods, demonstrating the same trend the transpiration chamber and the LAS, increasing the ET toward noon and decreasing at the end of the day in parallel to air temperature. However, the values achieving for each method are completely different. At 15:00 when the temperature is 25 °C, the relative humidity 35% and the wind speed 2.7 [m s^{-1}], the LAS reported the highest ET value of 0.5 [mm h^{-1}], while the lowest is those from the transpiration chamber: 0.06 [mm h^{-1}] and finally, the ET from the difference in the soil moisture is 0.18 [mm h^{-1}]. A possible cause of difference between ET computed from the LAS and the transpiration chamber is the LAS scintilliometer underestimation over the saturation zone, which may have led to an overestimation when the energy budget is closed (Equation 2).

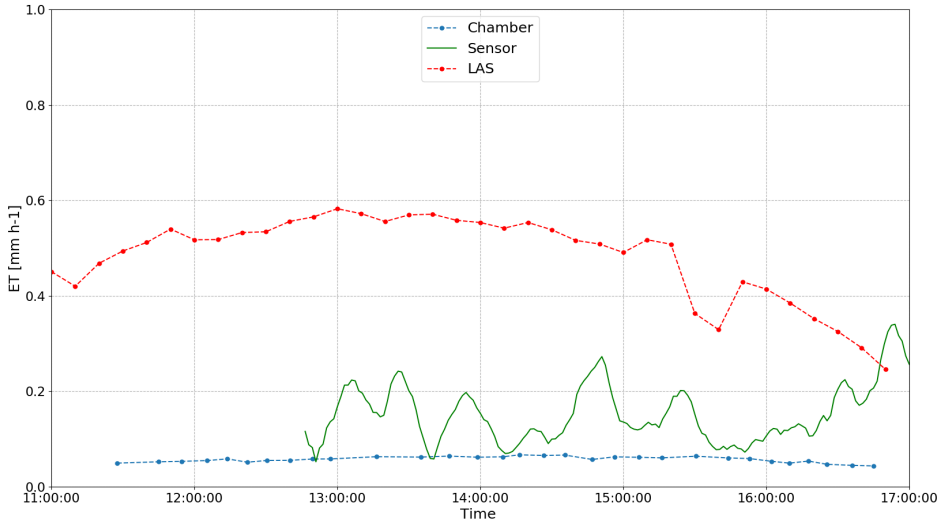

Figure 27. ET from the Scintillometer, sensors and transpiration chamber.

Another difference has been noticed between the transpiration chamber and the LAS measurement setups. It concerns specifically the net radiation measured by both devices (see Figure 28). Although they exhibit the same shape, respecting the diurnal cycle, the CNR4 provides systematically higher values (reaching 25%) than the NR-Lite. The location of each sensor can explain this difference. While the CNR4 radiometer is mounted at 1.4 m above the surface, the Radiometer NR-Lite of the chamber is located at 30 cm and close to a little shack. This position can cause some shades on the soil and affect (underestimate) *Rn* measurement.

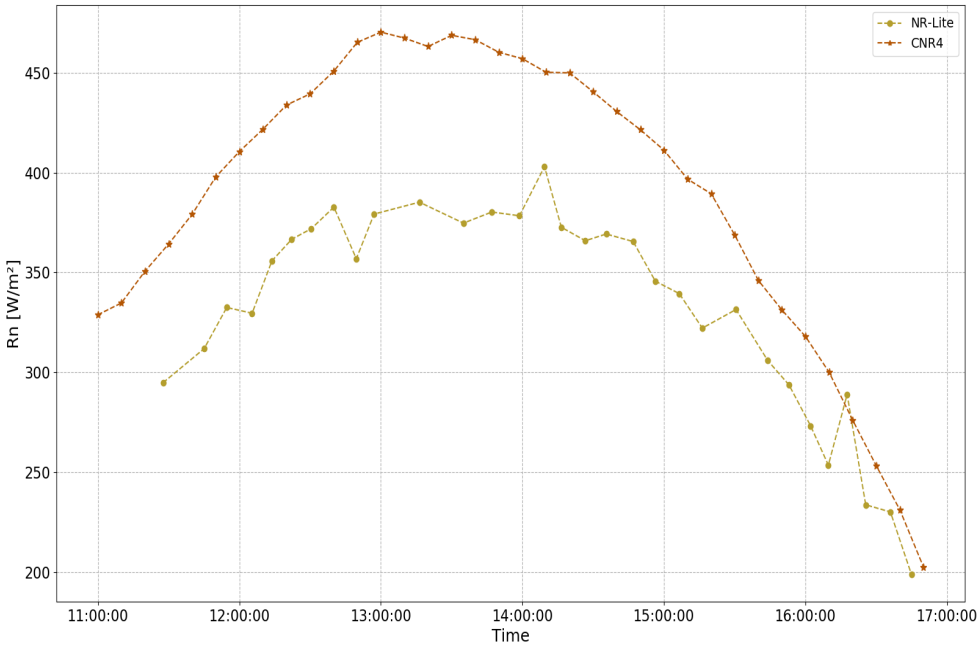

Figure 28. Net radiation measured by CNR4 and NR-Lite.

7. CONCLUSIONS

Evapotranspiration (ET) is one of process, which governs the behaviour of the Blue Green Solutions (BGS), and makes the link between the water balance and the energy budget. Consequently, it is necessary to assess it accurately and to understand its space-time variability at different scales. However, the measurement of this variable is not an easy task because it involves a large number of physical and meteorological parameters.

Different direct and indirect methods have been developed to estimate ET. For this study, three methods have been used: (i) an indirect method based on the water balance budget and using the moisture content difference measured by a network of wireless TDR sensors, (ii) a direct method measuring the flux of latent heat with a dynamic transpiration chamber, and (iii) an indirect method based on the energy budget and using a scintillometer to assess the sensible heat flux.

The water balance represents a good method to estimate ET but it is conditioned by the definition of dry seasons (without any precipitation, irrigation and runoff), where the meteorological conditions - especially the air temperature - force the loss of soil water by vapour water in the air. Thanks to the estimation of ET through the difference of the soil moisture, it was possible to analyse the daily characteristic fluctuation of water content. In the morning, as soon as the air temperature reaches the dew point water vapour begins to condense and can provide water to the soil. After, from the middle of the morning to the sunset, when temperature and radiation increase, ET process is supposed to reduce the soil moisture content. ET reaches its highest values at noon when the temperatures are high and when there is sufficient water into the soil. Then, it decreases during the afternoon, which is associated to a common ET process driven by solar radiation. Finally, ET remains constant during the night.

However, in winter there are additional factors, which can influence ET measurements, as low temperatures and wind, affecting the assumptions made on the hydric budget. Somme additional factors that may affect ET estimates are directly related to the water content measurement equipment (and particularly its resolution that could be not adapted to detect very small fluctuations), the sensor calibration and the adaptation of the Topp's Equation to the soil characteristics of the BGW.

Latent heat flux (Q_e) measured by the dynamic chamber is directly related to the net radiation. It increases simultaneously with net radiation and decreases when the atmospheric conditions are cloudy, as was shown during the August measurement campaigns. This can be attributed to the effects of the radiation on the air temperature, and consequently in the water vapour pressure, reducing the humidity.

The variation of the ET daily flux can be observed in detail thanks to the transpiration chamber. But this experimental setup has some adverse factors. First, the environmental conditions such as temperature and radiation within the chamber changes at the moment of putting it over the vegetation. Second, meteorological conditions as rainfall events and cloud cover can affect the measurements.

ET calculated from the sensors and the chamber at different locations of the BGW, do not indicate some clear trend related to the topography. However, the highest values of ET were

recorded in the lower point of the BGW, close to the drainage area, which indicates the strong influence of the moisture content for the ET process. This has also been verified during the measurements campaigns carried out at the end of the summer, when the lowest levels of ET and volumetric water content in the soil were reached. By contrast, at the end of the spring and the beginning of the summer, highest ET rates were recorded, explained by the raise of the temperatures, solar energy, vegetation growth and enough moisture content thanks to the last rainfalls events.

Finally, LAS scintillometer measurements seemed to not be reliable for different reasons. First, the low signal level measured at the receiver can represent a significant source of error as it may conduct to underestimate the sensible heat flux, and then overestimate the latent heat flux. The height of the device and the position of the beam in the saturation zone can also be mentioned to explain this inaccuracy. Here, the scintillation technique MOST used to deduce the sensible heat flux may not be valid.

8. PERSPECTIVES

ET measurements will be pursued in the coming months to collect data on a larger period of time, in different locations and weather conditions. The three methods will be deeply compared, to better understand the difference noticed between them during these first attempts, especially those presented above between the TDR sensors and the chamber.

The wireless sensors network will be used continuously on the BGW, and new campaigns with the dynamic transpiration chamber will be carried out in other locations. An in-depth analysis of the VWC data will be proposed to validate the measurements of dielectric constant through an analysis of uncertainty and sensibility with the aim of improving the estimation of ET.

A significant effort will be made to improve the results provided by the scintillometer. First it will be re-calibrated by the manufacturer (Kipp&Zonen) to be sure it is operational. Then several tests (concerning its location and the parameters introduced in the EVASION software) will be made to improve its functioning. The possibility to replace this LAS scintillometer by a laser scintillometer –more adapted to small distances- will be considered.

Concerning the ET estimation deduced from the energy budget, several improvement scan be planned. The first one concerns the soil heat flux. Indeed, it will be interesting to measure the daily temperature cycle from a single observation in order to apply the harmonic analysis method. This method allows to estimate the temperature gradient at several depths and any time, enabling the estimation of the soil heat flux, as Cohard et al. (2018) applied it in their calculation of the energy budget of an urban surface (asphalt concrete pavement). Moreover, an analysis about the thermal conductivity of the soil (k) should be undertaken. It will aim to take into account its spatial and temporal variability as a function of the soil properties.

From the collected data, a multifractal analysis will be conducted to characterize ET variability at different time and space scales. A particular attention will be paid to associate the spatial variability assessed by the VWC sensors and the average value measured by the transpiration chamber. The time variability will be assessed for VWC sensors and the scintillometer which are able to operate continuously. Multi-fractal allow an approach to the statistical physics of complex phenomena, and in particular the stochastic simulation of geophysical fields by exploiting their scaling laws. It is thus possible to describe the variability of intermittence outside the mean field and to study its extremes.

In this study, the not linear depth profile of the water in the soil was not taken into account with the TDR sensor. Nonetheless, this spatial variability could help to better understand the removal process of the water from the soil by the ET, as Guderle and Hildebrandt (2015) do reference in their study. In addition, the distinction between the water extraction by ET and the vertical water flux is one of the major challenges when water budget is applied, because these two events occur simultaneously during daytime

These experiments will conduct to develop a portable monitoring kit that can be used on other BGS and assess their thermo-hydric behavior. The data collected on the Green Wave and on additional sites where the portable monitoring setup will be applied, as well as those provided by the EVNATURB partners and friends will constitute a database devoted to BGS. This database aims to collect a wide range of situations in terms of soil/vegetation configuration, age, and climatic conditions. It will allow to follow these infrastructures and their related

performances over time by taking into account the possible degradation of materials. Moreover, the collected data will also be useful for model validation.

BIBLIOGRAPHIE

Acharya, D., Rani, A., Agarwal, S., Singh, V., 2016. Application of adaptive Savitzky–Golay filter for EEG signal processing. Perspect. Sci., Recent Trends in Engineering and Material Sciences 8, 677–679. https://doi.org/10.1016/j.pisc.2016.06.056

Ayata, T., Tabares-Velasco, P.C., Srebric, J., 2011. An investigation of sensible heat fluxes at a green roof in a laboratory setup. Build. Environ. 46, 1851–1861. https://doi.org/10.1016/j.buildenv.2011.03.006

Azami, H., Mohammadi, K., Bozorgtabar, B., 2012. An Improved Signal Segmentation Using Moving Average and Savitzky-Golay Filter. J. Signal Inf. Process. 03, 39–44. https://doi.org/10.4236/jsip.2012.31006

Barrio, E.P.D., 1998. Analysis of the green roofs cooling potential in buildings. Energy Build. 27, 179–193. https://doi.org/10.1016/S0378-7788(97)00029-7

Becker, D., Wang, D., 2011. Green Roof Heat Transfer and Thermal Performance Analysis. Carnegie Mellon University, Pittsburgh, USA.

Berretta, C., Poë, S., Stovin, V., 2014. Moisture content behaviour in extensive green roofs during dry periods: The influence of vegetation and substrate characteristics. J. Hydrol. 511, 374–386. https://doi.org/10.1016/j.jhydrol.2014.01.036

Besir, A.B., Cuce, E., 2018. Green roofs and facades: A comprehensive review. Renew. Sustain. Energy Rev. 82, 915–939. https://doi.org/10.1016/j.rser.2017.09.106

Brown, P., 2014. Basics of Evaporation and Evapotranspiration. Coll. Agric. Life Sci. Univ. Ariz.

Caird, M.A., Richards, J.H., Donovan, L.A., 2006. Nighttime Stomatal Conductance and Transpiration in C3 and C4 Plants. Plant Physiol. 143, 4–10. https://doi.org/10.1104/pp.106.092940

Cascone, S., Catania, F., Gagliano, A., Sciuto, G., 2018. A comprehensive study on green roof performance for retrofitting existing buildings. Build. Environ. https://doi.org/10.1016/j.buildenv.2018.03.052

Cenis, J.L., 1989. Temperature Evaluation in Solarized Soils by Fourier Analysis. Phytopathology 79, 506. https://doi.org/10.1094/Phyto-79-506

Chen, J., Jönsson, P., Tamura, M., Gu, Z., Matsushita, B., Eklundh, L., 2004. A simple method for reconstructing a high-quality NDVI time-series data set based on the Savitzky–Golay filter. Remote Sens. Environ. 91, 332–344. https://doi.org/10.1016/j.rse.2004.03.014

Cohard, J.-M., Rosant, J.-M., Rodriguez, F., Andrieu, H., Mestayer, P.G., Guillevic, P., 2018. Energy and water budgets of asphalt concrete pavement under simulated rain events. Urban Clim. 24, 675–691. https://doi.org/10.1016/j.uclim.2017.08.009

Coutts, A.M., Daly, E., Beringer, J., Tapper, N.J., 2013. Assessing practical measures to reduce urban heat: Green and cool roofs. Build. Environ. 70, 266–276. https://doi.org/10.1016/j.buildenv.2013.08.021

De Munck, C.S., Lemonsu, A., Bouzouidja, R., Masson, V., Claverie, R., 2013. The GREENROOF module (v7.3) for modelling green roof hydrological and energetic performances within TEB. Geosci Model Dev 6, 1941–1960. https://doi.org/10.5194/gmd-6-1941-2013

Evett, S.R., Agam, N., Kustas, W.P., Colaizzi, P.D., Schwartz, R.C., 2012. Soil profile method for soil thermal diffusivity, conductivity and heat flux: Comparison to soil heat flux plates. Adv. Water Resour. 50, 41–54. https://doi.org/10.1016/j.advwatres.2012.04.012

Fernández Gálvez, J., Verhoef, A., Barahona, E., 2007. Estimating soil water fluxes from soil water records obtained using dielectric sensors. Hydrol. Process. 21, 2785–2793. https://doi.org/10.1002/hyp.6494
Gagliano, A., Nocera, F., Detommaso, M., Evola, G., 2016. Thermal Behavior of an Extensive Green Roof: Numerical Simulations and Experimental Investigations. Int. J. Heat Technol. 34, S226–S234. https://doi.org/10.18280/ijht.34S206
Garcia, C.., Johnson, M.., Andraski, B.., Halford, K.., Mayers, C.., 2003. Portable Chamber Measurements of Evapotranspiration at the Amargosa Desert Research Site near Beatty, Nye County, Nevada, (No. 2008–5135). U.S. Geological Survey.
Guderle, M., Hildebrandt, A., 2015. Using measured soil water contents to estimate evapotranspiration and root water uptake profiles – a comparative study. Hydrol. Earth Syst. Sci. 19, 409–425. https://doi.org/10.5194/hess-19-409-2015
Guyot, A., Cohard, J.-M., Anquetin, S., Galle, S., Lloyd, C.R., 2009. Combined analysis of energy and water balances to estimate latent heat flux of a sudanian small catchment. J. Hydrol., Surface processes and water cycle in West Africa, studied from the AMMA-CATCH observing system 375, 227–240. https://doi.org/10.1016/j.jhydrol.2008.12.027
He, Y., Yu, H., Ozaki, A., Dong, N., Zheng, S., 2017. Influence of plant and soil layer on energy balance and thermal performance of green roof system. Energy 141, 1285–1299. https://doi.org/10.1016/j.energy.2017.08.064
HM&Co, 2017. Evnaturb – HM&Co [WWW Document]. Lab. Hydrol. Metereologie Complexité. URL https://hmco.enpc.fr/portfolio-archive/evnaturb/ (accessed 4.5.18).
Holmes, T.R.H., Owe, M., De Jeu, R.A.M., Kooi, H., 2008. Estimating the soil temperature profile from a single depth observation: A simple empirical heatflow solution: ESTIMATING THE SOIL TEMPERATURE PROFILE. Water Resour. Res. 44. https://doi.org/10.1029/2007WR005994
Jackson, T., Mansfield, K., Saafi, M., Colman, T., Romine, P., 2008. Measuring soil temperature and moisture using wireless MEMS sensors. Measurement 41, 381–390. https://doi.org/10.1016/j.measurement.2007.02.009
Kipp & Zonen B.V., 2015. LAS MkII Large Aperture Scintillometer 120.
Kolokotroni, M., Giridharan, R., 2008. Urban heat island intensity in London: An investigation of the impact of physical characteristics on changes in outdoor air temperature during summer. Sol. Energy 82, 986–998. https://doi.org/10.1016/j.solener.2008.05.004
Lagouarde, J., 2000. Analysis of the limits of the CT2-profile method for sensible heat flux measurements in unstable conditions. Agric. For. Meteorol. 105, 195–214. https://doi.org/10.1016/S0168-1923(00)00192-1
Lakshmi, V., Jackson, T.J., Zehrfuhs, D., 2003. Soil moisture-temperature relationships: results from two field experiments. Hydrol. Process. 17, 3041–3057. https://doi.org/10.1002/hyp.1275
Loustau, D., Cochard, H.H., Sartore, M., Guédon, M., 1991. Utilisation d'une chambre de transpiration portable pour l'estimation de l'évapotranspiration d'un sous-bois de pin maritime à molinie (Molinia coerulea (L) Moench). Ann. Sci. For. 48, 29–45.
Luo, C., Wang, Z., Sauer, T.J., Helmers, M.J., Horton, R., 2018. Portable canopy chamber measurements of evapotranspiration in corn, soybean, and reconstructed prairie. Agric. Water Manag. 198, 1–9. https://doi.org/10.1016/j.agwat.2017.11.024
Maksimovic, C., Stankovic, S., Liu, X., Lalic, M., 2013. Blue green dream project's solution for urban areas in the future. (Presented at the International science conference reporting for sustainability). Recici (Montenegro).

Malek, E., 1992. Night-time evapotranspiration vs. daytime and 24h evapotranspiration. J. Hydrol. 138, 119–129. https://doi.org/10.1016/0022-1694(92)90159-S
Malys, L., Musy, M., Inard, C., 2014. A hydrothermal model to assess the impact of green walls on urban microclimate and building energy consumption. Build. Environ. 73, 187–197. https://doi.org/10.1016/j.buildenv.2013.12.012
Marasco, D.E., Culligan, P.J., McGillis, W.R., 2015. Evaluation of common evapotranspiration models based on measurements from two extensive green roofs in New York City. Ecol. Eng. 84, 451–462. https://doi.org/10.1016/j.ecoleng.2015.09.001
McLeod, M.K., Daniel, H., Faulkner, R., Murison, R., 2004. Evaluation of an enclosed portable chamber to measure crop and pasture actual evapotranspiration at small scale. Agric. Water Manag. 67, 15–34. https://doi.org/10.1016/j.agwat.2003.12.006
Meijninger, W., n.d. The scintillation method.
Meijninger, W.M.., Green, A.E., Hartogensis, O.K., Kohsiek, W., Hoedjes, J.C.B., Zuurbier, R.M., De Bruin, H.A.R., 2002. Determination of Area-Averaged Water Vapour Fluxes with Large Aperture and Radio Wave Scintillometers over a Heterogeneous Surface – Flevoland Field Experiment. Bound.-Layer Meteorol. 105, 63–83. https://doi.org/10.1023/A:1019683616097
Mentens, J., Raes, D., Hermy, M., 2006. Green roofs as a tool for solving the rainwater runoff problem in the urbanized 21st century? Landsc. Urban Plan. 77, 217–226. https://doi.org/10.1016/j.landurbplan.2005.02.010
Moene, A.F., 2003. Effects of water vapour on the structure parameter of the refractive index for near-infrared radiation. Bound.-Layer Meteorol. 107, 635–653. https://doi.org/10.1023/A:1022807617073
Moorhead, J., Marek, G., Colaizzi, P., Gowda, P., Evett, S., Brauer, D., Marek, T., Porter, D., 2017. Evaluation of Sensible Heat Flux and Evapotranspiration Estimates Using a Surface Layer Scintillometer and a Large Weighing Lysimeter. Sensors 17, 2350. https://doi.org/10.3390/s17102350
Oberndorfer, E., Lundholm, J., Bass, B., Coffman, R.R., Doshi, H., Dunnett, N., Gaffin, S., Köhler, M., Liu, K.K.Y., Rowe, B., 2007. Green Roofs as Urban Ecosystems: Ecological Structures, Functions, and Services. BioScience 57, 823–833. https://doi.org/10.1641/B571005
O'Malley, C., Piroozfar, P., Farr, E.R.P., Pomponi, F., 2015. Urban Heat Island (UHI) mitigating strategies: A case-based comparative analysis. Sustain. Cities Soc. 19, 222–235. https://doi.org/10.1016/j.scs.2015.05.009
Ouldboukhitine, S.-E., Belarbi, R., Jaffal, I., Trabelsi, A., 2011. Assessment of green roof thermal behavior: A coupled heat and mass transfer model. Build. Environ. 46, 2624–2631. https://doi.org/10.1016/j.buildenv.2011.06.021
Poë, S., Stovin, V., Berretta, C., 2015. Parameters influencing the regeneration of a green roof's retention capacity via evapotranspiration. J. Hydrol. 523, 356–367. https://doi.org/10.1016/j.jhydrol.2015.02.002
Ramier, D., Chollet, J., Berthier, E., Sabre, M., Tétard, Y., Flori, J.-P., Bouyer, J., 2015. Mesure de l'évapotranspiration à petite échelle spatiale : applications aux toitures végétalisées.
Ren, R., Ma, J., Cheng, Q., Zheng, L., Guo, X., Sun, X., Ren, R., Ma, J., Cheng, Q., Zheng, L., Guo, X., Sun, X., 2017. An Investigation into the Effects of Temperature Gradient on the Soil Water–Salt Transfer with Evaporation. Water 9, 456. https://doi.org/10.3390/w9070456

Schertzer, D., Lovejoy, S., 2011. Multifractals, generalized scale invariance and complexity in geophysics. Int. J. Bifurc. Chaos 21, 3417–3456. https://doi.org/10.1142/S0218127411030647

Schwärzel, K., Menzer, A., Clausnitzer, F., Spank, U., Häntzschel, J., Grünwald, T., Köstner, B., Bernhofer, C., Feger, K.-H., 2009. Soil water content measurements deliver reliable estimates of water fluxes: A comparative study in a beech and a spruce stand in the Tharandt forest (Saxony, Germany). Agric. For. Meteorol. 149, 1994–2006. https://doi.org/10.1016/j.agrformet.2009.07.006

Stacheder, M., Koeniger, F., Schuhmann, R., 2009. New Dielectric Sensors and Sensing Techniques for Soil and Snow Moisture Measurements. Sensors 9, 2951–2967. https://doi.org/10.3390/s90402951

Stanic, F., Versini, P.A., Tchiguirinskaia, I., Schertzer, D., Cui, Y.J., Delage, P., 2018. Analysis of green roof's water balance components using Universal Multifractal (UM) framework.

Stannard, D.I., 1988. Use of a hemispherical chamber for measurement of evapotranspiration (No. 88–452). U.S. Geological Survey.

Stefferud, S., 2016. Soil Moisture Measurements and Evapotranspiration in Extensive Green Roofs. Norwegian University of Science and Technology.

Tabares, P.C., Srebric, J., 2012. A heat transfer model for assessment of plant based roofing systems in summer conditions. Build. Environ. 49, 310–323. https://doi.org/10.1016/j.buildenv.2011.07.019

Tan, C.L., Tan, P.Y., Wong, N.H., Takasuna, H., Kudo, T., Takemasa, Y., Lim, C.V.J., Chua, H.X.V., 2017. Impact of soil and water retention characteristics on green roof thermal performance. Energy Build. 152, 830–842. https://doi.org/10.1016/j.enbuild.2017.01.011

Tie, Q., Hu, H., Tian, F., Holbrook, N.M., 2018. Comparing different methods for determining forest evapotranspiration and its components at multiple temporal scales. Sci. Total Environ. 633, 12–29. https://doi.org/10.1016/j.scitotenv.2018.03.082

Valayamkunnath, P., Sridhar, V., Zhao, W., Allen, R.G., 2018. Intercomparison of surface energy fluxes, soil moisture, and evapotranspiration from eddy covariance, large-aperture scintillometer, and modeling across three ecosystems in a semiarid climate. Agric. For. Meteorol. 248, 22–47. https://doi.org/10.1016/j.agrformet.2017.08.025

Versini, P.A., Gires, A., Fitton, G., Tchiguirinskaia, I., Schertzer, D., 2018. ENPC Blue Green Wave: a Blue Green Dream pilot site to assess multifunctional aspect of green infrastructures. Houille Blanche.

Versini, P.-A., Gires, A., Tchiguirinskaia, I., Schertzer, D., 2016. Toward an operational tool to simulate green roof hydrological impact at the basin scale: a new version of the distributed rainfall-runoff model Multi-Hydro. Water Sci. Technol. 74, 1845–1854. https://doi.org/10.2166/wst.2016.310

Wadzuk, B.M., Schneider, D., Feller, M., Traver, R.G., 2013. Evapotranspiration from a Green-Roof Storm-Water Control Measure. J. Irrig. Drain. Eng. 139, 995–1003. https://doi.org/10.1061/(ASCE)IR.1943-4774.0000643

Wang, Y., Bakker, F., de Groot, R., Wörtche, H., 2014. Effect of ecosystem services provided by urban green infrastructure on indoor environment: A literature review. Build. Environ. 77, 88–100. https://doi.org/10.1016/j.buildenv.2014.03.021

Yang, J., Mohan Kumar, D. llamathy, Pyrgou, A., Chong, A., Santamouris, M., Kolokotsa, D., Lee, S.E., 2018. Green and cool roofs' urban heat island mitigation potential in tropical climate. Sol. Energy 173, 597–609. https://doi.org/10.1016/j.solener.2018.08.006

Yee, M.S., Pauwels, V.R.N., Daly, E., Beringer, J., Rüdiger, C., McCabe, M.F., Walker, J.P., 2015. A comparison of optical and microwave scintillometers with eddy covariance derived surface heat fluxes. Agric. For. Meteorol. 213, 226–239. https://doi.org/10.1016/j.agrformet.2015.07.004